HHS Public Access

Author manuscript

Nature. Author manuscript; available in PMC 2022 July 19.

Published in final edited form as:

Nature. 2022 January ; 601(7894): 637–642. doi:10.1038/s41586-021-04295-4.

Ageing exacerbates ribosome pausing to disrupt cotranslational proteostasis

Kevin C. Stein[1], **Fabián Morales-Polanco**[1], **Joris van der Lienden**[1], **T. Kelly Rainbolt**[1], **Judith Frydman**[1,2,*]

[1]Department of Biology, Stanford University, Stanford, California, 94305, USA

[2]Department of Genetics, Stanford University, Stanford, California, 94305, USA

Abstract

Ageing is accompanied by a decline in cellular proteostasis, which underlies many age-related protein misfolding diseases[1,2]. Yet, how ageing impairs proteostasis remains unclear. As nascent polypeptides represent a substantial burden on the proteostasis network[3], we hypothesized that altered translational efficiency during ageing could help drive proteostasis collapse. Here, we show that ageing alters the kinetics of translation elongation in both *C. elegans* and *S. cerevisiae.* Ribosome pausing was exacerbated at specific positions in aged yeast and worms, including polybasic stretches, leading to increased ribosome collisions known to trigger Ribosome-associated Quality Control (RQC)[4–6]. Notably, aged yeast cells exhibited impaired clearance and increased aggregation of RQC substrates, indicating ageing overwhelms this pathway. Indeed, long-lived yeast mutants reduced age-dependent ribosome pausing, and extended lifespan correlated with greater flux through the RQC pathway. Further linking altered translation to proteostasis collapse, we found that nascent polypeptides exhibiting age-dependent ribosome pausing in *C. elegans* were strongly enriched among age-dependent protein aggregates. Remarkably, ageing increased the pausing and aggregation of many proteostasis components, which could initiate a detrimental cycle of proteostasis collapse. We propose that increased ribosome pausing, leading to RQC overload and nascent polypeptide aggregation, critically contributes to proteostasis impairment and systemic decline during ageing.

Accurately generating the nascent proteome represents a substantial burden on proteostasis networks[3,7]. Compared to mature proteins, partially-folded nascent polypeptides are metastable and more susceptible to misfolding[8,9]. During translation elongation, the speed of the ribosome is positionally variable[10], and these local changes impact co-translational proteostasis[11]. Transient elongation slowdowns facilitate co-translational

[*]**Correspondence and requests for materials** should be addressed to J.F. jfrydman@stanford.edu.

Author contributions K.C.S. and J.F. designed the study. K.C.S. performed all experiments and computational analyses, with assistance from F.M-P., JL., and T.K.R. in carrying out the yeast reporter immunoblot and microscopy experiments. K.C.S. and J.F. wrote the manuscript with input from all authors.

Competing interests The authors declare no competing interests.

Additional information

Supplementary information is available for this paper.

Code availability All customized python or R scripts used for data processing and analysis are available upon request.

protein folding[12–15], assembly[16], organelle targeting[17,18], and chaperone recruitment[19]. However, prolonged slowdowns can lead to ribosome collisions and degradation of the nascent polypeptide and transcript[4–6,20–22]. Disrupting translation kinetics or co-translational processing leads to aggregation of nascent proteins, impaired cellular fitness, and neurodegeneration[23–33]. Although proteostasis collapse is also a hallmark of ageing[1,34,35], it remains unknown whether disrupting the tight balance between translation elongation and co-translational flux is involved (Fig. 1a).

We used Ribo-Seq to examine whether ageing alters translation elongation in two well-established models of post-mitotic ageing: the nematode *C. elegans* and budding yeast *S. cerevisiae* (Fig. 1b, Extended Data Fig. 1a). Validating our datasets, we observed age-related reduction of translation initiation in both organisms, which was associated with lower production of translation components, such as ribosomal proteins, and is consistent with previous studies[36–41] (Extended Data Fig. 1b–h, 2a–g). We also confirmed ageing increased translation of genes involved in stress responses, such as *GCN4* in yeast (Extended Data Fig. 1i).

To analyze ribosome pausing, we calculated a pause score for each position of a coding sequence relative to the whole transcript. The cumulative distribution of pause scores across the transcriptome showed no global age-related changes (Fig. 1c), similar to previous observations[42]. Average amino acid pause scores also showed negligible differences with age (Extended Data Fig. 1j–k, 2h–i). This indicates that the metabolic changes of ageing do not cause a systemic change in overall elongation pausing. However, hypothesizing that ageing might cause specific alterations in translation elongation, we adapted a statistical metric[19] to probe elongation pausing during ageing at single codon resolution. To validate this approach, we used Ribo-Seq of yeast treated with 3-Amino-1,2,4-triazole (3-AT)[43,44], which inhibits histidine biosynthesis and causes ribosome pausing at histidine positions ([43,44] and Extended Data Fig. 3a). Our approach identified statistically significant ribosome pausing and found that only histidine was enriched among these sites (Extended Data Fig. 3b).

Having validated our metric for detecting specific changes in ribosome pausing, we used our Ribo-Seq data to identify positions with significant ageing-related changes in translation kinetics (Fig. 1d). Notably, in both worms and yeast, these changes included thousands of positions with significantly increased ribosome occupancy during ageing, incrementally increasing as the organism aged (Fig. 1e). We termed these positions age-dependent ribosome pause sites (Supplementary Table 1), representing sites with increased ribosome slowdown during ageing. These sites were enriched in genes involved in proteostasis and translation (Extended Data Fig. 3c–d, Supplementary Table 2), suggesting multiple mechanisms by which altered elongation may impair proteostasis (see Supplementary Discussion). Moreover, transcripts with age-dependent pausing were enriched among polypeptides that are co-translationally ubiquitinated (Extended Data Fig. 3e), indicating ageing may disrupt the biogenesis of proteins that are metastable even in young cells.

To investigate the basis of age-dependent ribosome pausing in yeast, we analyzed the sequence specificity of pauses[45]. We found significant positional enrichment of certain

amino acids, with Pro and the basic residues Arg and Lys being enriched in multiple ribosomal active site positions (Fig. 2a–b). Examining codon frequency in age-dependent pause sites showed that most codons for Arg, Glu, and Pro were enriched (Extended Data Fig. 3f). This indicates that amino acid properties and not codon optimality primarily determine age-dependent pausing. We also used an alternative approach to examine amino acid enrichment by calculating the average pause score for all possible 8,000 tripeptide motifs[46]. This strategy again identified a particular association of Arg, Lys, and Pro with increased ribosome pausing during ageing (Extended Data Fig. 3g–i).

Prolonged pausing leads to ribosome collisions, which are detrimental and must be cleared by the RQC pathway[4,20]. We noted that similar amino acid residues associated with age-dependent pausing lead to formation of collided disomes and trisomes (Extended Data Fig. 4a and [47]). As ageing further compromises decoding these residues, such as at a Trp codon in *HAT2* (Extended Data Fig. 4b–c), we examined whether ageing impacts the likelihood of ribosome collisions. We identified the position in each transcript where disomes were most enriched over monosomes in young cells[47] and found that ageing exacerbated ribosome collisions at these sites (Extended Data Fig. 4d). Similarly, we found ageing exacerbated ribosome collisions at codon pairs previously shown to slow translation elongation[48] and tripeptide motifs associated with ribosome collisions[47] (Extended Data Fig. 4e–h). Polybasic motifs such as RKK showed both increased ribosome collisions and pausing. Collectively, these observations indicate that ageing alters translation kinetics and exacerbates ribosome pausing and collisions at many positions in the yeast translatome, but particularly at motifs known to cause slowdowns in young organisms, such as polybasic stretches[20].

We next wanted to dissect how ageing impacts translation of polybasic regions. We identified Arg/Lys repeats of increasing length within the yeast transcriptome (Supplementary Table 3) and used previous Ribo-Seq data from monosome- or disome-protected mRNA[47] to establish expected patterns of ribosome pausing and collisions. Longer polybasic stretches caused increased ribosome pausing, a shift in peak ribosome occupancy after the polybasic stretch enters the ribosome, and increased lagging ribosome peaks indicative of disome/trisome pileup (Extended Data Fig. 5a–b). We then determined how ageing affected ribosome occupancy at polybasic regions in yeast. Compared to young cells, aged cells showed more severe pausing, and an additional ribosome peak was observed ~10 codons upstream of the main pause site, a signature of ribosome collision[4,20,43,44,47] (Fig. 2c–d, Extended Data Fig. 5c–e). Moreover, the age-dependent increase in pausing and ribosome collisions was enhanced for longer polybasic tracts. We also observed age-dependent pausing and collisions at polybasic sites without consecutive Arg/Lys, e.g. the Hsp40 chaperone *SIS1* (Extended Data Fig. 5f). The polybasic tract in *YTM1* further highlights the impact of ageing: although disome profiling[47] showed ribosomes collide at this region even in young cells, monosome footprinting only detects an upstream ribosome peak in aged cells (Fig. 2e–f). Thus, ageing sufficiently increases the frequency of ribosome collisions to make them directly detectable without isolating disomes.

Several factors in the RQC pathway help resolve collided ribosomes and degrade the nascent protein[4–6,20,47,49–51], including recognition by Hel2, C-terminal alanine and threonine (CAT) tail formation by Rqc2, and ubiquitination by Ltn1/Rkr1[6,21,52–60]. Disrupting this

pathway leads to toxic aggregation of stalled nascent chains[29,30]. To test whether the age-dependent increase in ribosome pausing and collisions affects the handling of stalled nascent chains, we used RQC reporters containing polybasic stretches of either 12 Arg or Lys (R12 or K12) inserted between GFP and RFP[6,22]. These inserts cause ribosome pausing and efficient degradation of stalled polypeptides in young cells[22]. By contrast, aged cells exhibited dramatic accumulation of truncated, stalled nascent chains (Fig. 3a), which did not result from changes in media composition or metabolism during yeast chronological ageing (Extended Data Fig. 6a–c).

As further validation that ageing decreases the ability to clear stalled RQC substrates, we used RQC mutants. Ageing exacerbated the levels of stalled truncated products seen in *ltn1Δ* and *rqc2Δ* cells (Fig. 3a), suggesting that age-dependent accumulation of stalled polypeptides does not simply result from impaired RQC activity. Notably, aged *ltn1Δ* cells showed increased formation of high molecular weight (HMW) aggregates of the stalling reporters but not the GFP-RFP control, and decreased CAT-tailed products presumably by incorporation into aggregates (Fig. 3a, Extended Data Fig. 6a). Similarly, using fluorescent microscopy, we found ageing strongly increased formation of GFP+/RFP- puncta for both polybasic reporters, which we validated by immunoblot using a FLAG-His3 reporter (Fig. 3b, Extended Data Fig. 6d–g). Although formation of GFP+/RFP- puncta increased in aged *rqc2Δ* cells, it was less than WT and *ltn1Δ* cells, suggesting that CAT tails promote, but are not necessary for, age-dependent aggregation of stalled truncated polypeptides.

We next extended these findings to endogenous proteins that showed increased pausing in aged cells. First, we utilized two fusion constructs of *YTM1* having either an N-terminal or C-terminal GFP tag to differentiate between co- and post-translational products. In contrast to young cells, ageing increased the production of co-translational truncated products, which were distinct from post-translational products (Extended Data Fig. 7a). Moreover, ageing increased GFP+ puncta formation when *YTM1* was N-terminally tagged, but not C-terminally tagged, in both WT and *ltn1Δ* cells (Extended Data Fig. 7b). We also observed accumulation of co-translational truncated products with age for N-terminally GFP-tagged *HAT2* (Extended Data Fig. 7c). This confirms that ageing impairs RQC processing of stalled polypeptides.

We further used *hel2Δ* cells to dissect how ageing impacts RQC initiation[20,51]. Although aged *hel2Δ* cells showed increased GFP+/RFP- puncta formation like the other RQC mutants, there was also a significant increase of GFP+/RFP+ puncta using the stalling reporters (Fig. 3b, Extended Data Fig. 6d–f, 7d). As we also observed increased production of full-length reporter protein in aged cells of all genotypes (Fig. 3a), we hypothesized that ageing may cause greater bypass of stalling sequences. We used Ribo-Seq of young and aged cells containing the K12 stalling reporter and found that ageing increased ribosome occupancy at the 3’ end of the transcript (Extended Data Fig. 7e), similar to findings in mice[61]. These data suggest that ageing has pleiotropic effects on RQC, disrupting both the resolution of stalled ribosomes and processing of stalled polypeptides.

Upon linking ageing with increased ribosome pausing/collisions and dysfunctional RQC, we next asked whether clearance of RQC substrates impacts lifespan (Fig. 3c). We compared

two genome-wide screens: one measured the chronological lifespan of each strain in the yeast deletion collection[62], and the other quantified clearance of the GFP-R12 RQC substrate[6]. We grouped yeast strains based on GFP-R12 abundance, which acts as a proxy for RQC flux: strains with high GFP levels, such as the RQC mutants, have reduced capacity to clear stalled nascent chains. We found that strains with the highest GFP-R12 abundance had shortened lifespans, whereas strains with the lowest GFP-R12 levels had the longest lifespans (Fig. 3c), suggesting that RQC flux impacts longevity. Moreover, compared to strains with impaired RQC flux, we found increased RQC flux in yeast strains that are chronologically long-lived – including strains not involved in the TOR pathway – and strains having extended replicative lifespan (Extended Data Fig. 8a). These analyses link defective clearance of stalled nascent polypeptides with accelerated ageing.

To further examine the relationship between translation elongation and lifespan, we used cells deleted for *SCH9*, the ortholog of mammalian S6K and a substrate of the TOR pathway[34]. Mutation of this component is a highly conserved means of extending lifespan[63,64]. We first found that *sch9Δ* cells significantly mitigated the age-dependent pausing observed in WT cells (Extended Data Fig. 8b–c). Moreover, sites with greater pausing in aged WT cells versus aged *sch9Δ* cells showed enrichment of Arg, Pro, Gly, and Lys (Extended Data Fig. 8d), indicating that loss of Sch9 reduces pausing at these residues. There was also marked reduction in both pausing and collisions at polybasic tracts in aged *sch9Δ* cells (Fig. 3d, Extended Data Fig. 8e–f). Using stalling reporters, aged *sch9Δ* cells exhibited less accumulation of truncated polypeptides and abrogated their aggregation during ageing (Fig. 3e, Extended Data Fig. 8g–h). We also found that ageing reduced translation of several RQC components, which was attenuated in *sch9Δ* cells (Extended Data Fig. 8i). Notably, *LTN1* translation was not changed in *sch9Δ* cells. Collectively, our data suggest that the age-dependent increase in ribosome pausing overwhelms the RQC pathway, contributing to dysfunctional co-translational proteostasis and the regulation of lifespan (Fig. 3f).

Extending our analysis to *C. elegans*, we also found enrichment of certain residues at age-dependent pause sites (Fig. 4a–b, Extended Data Fig. 9a–f). In particular, Arg was enriched in these sites, independent of codon usage, and in tripeptide motifs having increased pausing during ageing. Moreover, we found a length-dependent increase in ribosome pausing in aged worms at polybasic motifs: pausing increased at regions of four consecutive K/R and was even higher at five and six consecutive K/R (Fig. 4c, Extended Data Fig. 9g). Increased pausing at motifs of six K/R was accompanied by the signature upstream peak of ribosome collisions, as illustrated at a five K/R stretch in *tag-342* (Fig. 4c–d). Thus, exacerbated ribosome pausing at polybasic regions leading to increased ribosome collisions is a conserved feature of ageing in both yeast and worms.

We next examined the relationship between age-dependent ribosome pausing and protein aggregation during worm ageing[37,65]. Remarkably, we found a strong association, with genes having age-dependent ribosome pauses being over-represented about three-fold among proteins that aggregate with age (Fig. 4e, Extended Data Fig. 10a). Furthermore, proteins that aggregate in aged worms were enriched for polybasic motifs, particularly in proteins with age-dependent pausing (Extended Data Fig. 10b). We also found that

age-dependent pausing and aggregation affected many proteins involved in translation and proteostasis (Fig. 4f, Extended Data Fig. 10c, Supplementary Table 2). For instance, all nine aminoacyl tRNA synthetases showing age-dependent pausing also aggregated during ageing (Fig. 4g, Extended Data Fig. 10d). In addition, several RQC components have reduced translation and increased aggregation during worm ageing (Extended Data Fig. 10e–f). This likely exacerbates the enhanced load on this pathway from increased ribosome collisions and disrupts co-translational proteostasis.

Our data establish that altered ribosome pausing is a crucial conductor of the ageing process, providing a link to protein aggregation and proteostasis dysfunction. The age-dependent increase in ribosome pausing is conserved between worms and yeast, and is associated with increased ribosome collisions, decreased flux through the RQC pathway, and ensuing aggregation of truncated nascent proteins. We propose that this connection between age-related pausing and aggregation of nascent chains precipitates a cycle of dysfunction during ageing (Supplementary Discussion).

Elongation rate alterations likely disrupt several co-translational pathways, including folding and organelle targeting[11,17–19,23]. Here, we focused on the interplay between ribosome pausing and RQC. Highlighting the importance of this interplay, increased stalling[32], or dysfunctional RQC[33], can cause neurodegeneration. There is likely a delicate balance between ribosome slowdowns that facilitate protein folding/targeting and slowdowns that lead to ribosome collisions and trigger RQC. Our data suggest that ageing disrupts this balance by causing greater ribosome pausing (Fig. 4h), particularly at polybasic stretches. We propose that in younger organisms, pausing at these regions seldom causes ribosome collisions that trigger RQC, in agreement with RQC not regulating basal positively-charged protein expression[66]. As a result, young organisms presumably have adequate capacity to handle infrequent strong ribosome pauses. By contrast, impaired resolution of ribosome pausing in aged organisms increases the frequency of ribosome collisions, thereby overwhelming RQC. Altered translation kinetics during ageing might also disrupt co-translational folding of nascent polypeptides and cause additional aggregation or stoichiometry imbalances that further disrupt proteostasis (Supplementary Discussion). Such implications demonstrate that ribosome pausing is likely a critical driver of age-related proteostasis decline associated with many late-onset misfolding diseases.

Methods

Strains and growth conditions.

The Bristol N2 strain of *C. elegans* was grown at 20°C on nematode growth medium agar plates seeded with *Escherichia coli* strain OP50, following standard methods[67]. All yeast experiments were performed using derivatives of BY4741 (MATa *his3Δ1 leu2Δ0 met15Δ0 ura3Δ0*). Ribo-Seq experiments used diploid BY4743 (WT) and homozygous *sch9Δ/sch9Δ* (YSC6275–201917395), which were obtained from GE Healthcare Dharmacon. For immunoblotting and microscopy experiments, haploid strains of WT, *ltn1Δ*, *rqc2Δ, hel2Δ, and sch9Δ* were from the Yeast Knockout Collection[68]. Strains from the N-terminally GFP tagged seamless collection[69] as well as from the C-terminally GFP tagged clone collection[70] were used for the *YTM1* and *HAT2* experiments. Yeast cells were grown at

30°C in variations of synthetic complete (SC) media[62] with fivefold excess of nutrients to compensate for strain auxotrophies.

Plasmid and yeast strain construction.

Ribosome pausing reporter plasmids were derived from gifts from Onn Brandman[52] and Toshifumi Inada[22]. The *PGK1* promoter was amplified using oligonucleotides 5'GCGGAGCTCTGTTTGCAAAAAGAACAAAAC and 5'GCGTCTAGATGTTTTATATTTGTTGTAAAAAG, digested with SacI/XbaI, and ligated to create p416PGK-GFP-R12-FLAG-HIS3 and p416PGK-GFP-K12(AAA)-FLAG-HIS3. Correct clones were confirmed by colony PCR and sequencing. Experiments using GFP-R12-RFP and GFP-K12-RFP pausing reporters were performed after integrating these reporters into yeast. First, RFP was amplified from pTDH3-GFP-R12-RFP[52] using oligonucleotides 5'GCGACTAGTATGGTGAGCGAGCTGATTAAG and 5'GCGGAATTCTTATCTGTGCCCCAGTTTG, digested with SpeI/EcoRI-HF, and ligated to replace the FLAG-HIS3 in the plasmids above to create p416PGK-GFP-R12-RFP and p416PGK-GFP-K12(AAA)-RFP. A XbaI/ClaI digest was used to clone the reporter into pAG306GPD-ccdB-chrI, a gift from Dan Gottschling (Addgene plasmid #41894)[71]. These constructs were then digested with NotI and transformed into yeast cells using standard methods and selected on SC-ura. Correct clones were confirmed by colony PCR, sequencing, and microscopy.

To construct *ltn1Δ* strains with integrated *YTM1* GFP fusions, *LTN1* was deleted from the knock-in strains via standard PCR-based homologous recombination. The *YTM1-GFP ltn1Δ* strain was constructed by replacing *LTN1* with *LEU2* using a cassette amplified from plasmid GTL-g (Addgene plasmid #81099) with oligonucleotides 5'GATTATGCCCCAACATGGAAAACTGAAAAATATTGATGAAGCGAGTCTGTAGGCGAACCTAACCGG and 5'TTTCCAGAATATCCGGGTGATGGGCTGGATTGGCAAGGTATTATATGAAGATTGTTCTACCATTCACAACTATAT. Similarly, the *GFP-YTM1 ltn1Δ* strain was constructed by replacing *LTN1* with *URA3* using a cassette amplified from plasmid pSH100 (Addgene plasmid #45930) with oligonucleotides 5'GATTATGCCCCAACATGGAAAACTGAAAAATATTGATGAAGCGAGCCACAGCTTTTCAATTCAATTCATCA and 5'TTTCCAGAATATCCGGGTGATGGGCTGGATTGGCAAGGTATCCTGATGCGGTATTTTCTCCTTA. Both cassettes were amplified, separated by electrophoresis, gel purified and transformed into yeast cells using the lithium acetate method. Correct transformants were verified by standard PCR using the oligonucleotides LTN1-VF: 5' TCCGTTTTGGATTCGTTGGAGT, LTN1-VR: 5' ACCGCCAAGCAGAAAATCC, LEU2-VF: 5' AGCACGAGCCTCCTTTACCT, and URA3-VF: 5' CGAATGCACACGGTGTGGT.

Ribo-Seq.

For *C. elegans* samples, after passaging for at least three generations, age-synchronized populations of L1 larvae were obtained and grown to the L4 larval stage (Day 0). The plates of L4 animals were then washed and the collected animals were transferred to plates containing 50 μg/mL 5-fluoro-2'-deoxyuridine (FUdR; Millipore Sigma) at ~1,000

worms per plate. Animals were carefully monitored to ensure adequate bacteria was in constant supply, adding concentrated stocks of bacteria as necessary. At each of the indicated ages, ~40,000 adult worms were collected by quickly washing subsets of plates into microcentrifuge tubes using modified lysis buffer (20 mM Tris-HCl pH 7.5, 140 mM KCl, 1.5 mM $MgCl_2$), followed by a short centrifugation (0.3 g at room temperature for 10 sec) that minimized the number of eggs and bacteria that pelleted with the animals. Supernatant from each tube was then aspirated and pelleted animals were dripped into liquid nitrogen. Lysis was performed by combining 1 mL of lysis buffer containing twice the concentration of DTT, cycloheximide (CHX), and Triton X-100 (20 mM Tris-HCl pH 7.5, 140 mM KCl, 1.5 mM $MgCl_2$, 1 mM DTT, 200 μg mL^{-1} CHX, 2% Triton X-100) to compensate for the approximate volume of lysis buffer that remained when harvesting the animals. Worms were then pulverized using a MM-301 mixer mill at 20 Hz for 1 min, with lysate being thawed in a room temperature water bath at room temperature and centrifuged at 15,000 g at 4°C for 10 min. After quantifying RNA concentration, 200 μg RNA was incubated for 45 min with 0.75 μl 100 U $μl^{-1}$ RNase I (Ambion), with another 200 μg RNA being kept on ice undigested to use for polysome profiles. Sucrose gradient centrifugation and fractionation were then performed as described previously[17]. Total RNA was extracted from the digested 80S fraction using the hot SDS-phenol-chloroform method, 20–35 nucleotide RNA footprints were isolated, ribosomal RNA was removed using the Ribo-Zero kit (Illumina), with remaining library preparation steps described elsewhere[72]. Barcoded samples were pooled and sequenced with a HiSeq 4000 (Illumina). For yeast samples, overnight cultures were diluted to an OD_{600} of 0.05 in 500 mL SC media and grown at 30°C. Part of each culture was harvested as Day 0 cells at an OD_{600} of ~0.7, with the remaining culture placed back at 30°C for 48 and 96 hours for harvesting Day 2 and Day 4 cells, respectively. All cells were harvested by vacuum filtration and freezing in liquid nitrogen. Lysis was performed by combining 2 mL of lysis buffer (20 mM Tris-HCl pH 7.5, 140 mM KCl, 1.5 mM $MgCl_2$, 0.5 mM DTT, 100 μg mL^{-1}, 1% Triton X-100) frozen in liquid nitrogen with cell pellets, with the remaining steps of lysis and library preparation following that of worms described above.

Data processing and pause score calculation.

Demultiplexed sequencing reads were trimmed of adaptor sequences using Cutadapt v1.4.2, followed by removal of the 5' nucleotide using FASTX-Trimmer. Reads that mapped to ribosomal RNAs using Bowtie v1.0.0 (http://bowtie-bio.sourceforge.net/index.shtml)[73] were removed. Remaining reads were aligned to reference libraries that consisted of coding sequences containing 21 nucleotides flanking upstream of the start codon and downstream of the stop codon, or the entire transcript sequence including untranslated regions. The *C. elegans* library consisted of the longest transcript of 20,222 genes (ce11 / WBcel235), and the yeast library consisted of 5,793 ORFs (sacCer3 / R64–1-1) that excluded ORFs characterized as dubious or that overlapped with other genes. Bowtie v1.0.0 alignment of sequencing reads to these libraries used the following parameters to allow for two mismatches and keep only uniquely mapped reads for further analysis: -y -a -m 1 -v 2 --norc --best --strata. For each footprint length, customized python scripts were used to sum reads at each nucleotide. Metagene analysis was performed separately on each fragment length, and lengths that did not exhibit the characteristic 3-nucleotide periodicity were removed.

Remaining reads had a nucleotide offset empirically determined from the 5' end of each fragment length, using the characteristic large ribosome density at the start codon, so that each read was assigned to the first A-site nucleotide. Nucleotide reads at each codon were then summed and used for all additional analysis.

To analyze gene expression, reads were summed for each gene after excluding the first 20 and last 20 sense codons, followed by calculating tpm. Statistical significance was calculated using DESeq2[74] for genes with greater than 64 reads in each biological replicate. Pause scores at each codon position in a transcript were calculated by dividing the number of reads at that position by the expected number of reads, which was defined as the average number of reads across the internal part of the transcript, i.e. excluding the first 20 and last 20 sense codons. Mathematically:

$$\text{Pause score} = \frac{RRij}{\frac{\sum_{i=21}^{k-20} RRij}{k-40}}$$

where RR is the number of ribosomal reads at position i of gene j that has length k codons.

Age-dependent pause site identification.

To identify positions where ribosome pausing was increased during ageing, we included genes that had an average sequencing coverage of ≥ 0.5 reads per codon (calculated as above), and ≥ 64 total reads in each replicate, which included 7,200 *C. elegans* genes and 4,082 yeast genes. Next, we adapted a strategy we used previously[19] that used two-tailed Fisher's exact tests to identify positions where statistically significant changes in ribosome pausing between the young (Day 1 worms and Day 0 yeast) and old (Day 12 worms and Day 4 yeast) samples. Briefly, reads at each position and for each transcript were averaged between replicates and rounded to the nearest integer. At each position of a transcript, 2 x 2 contingency tables were created to perform a two-tailed Fisher's exact test to compare the ratio of reads in the young and aged fractions at a given position to the ratio at all other positions in that transcript (i.e. the summed reads in each fraction for the entire transcript minus the position of interest). In other words, this compares the observed ratio of ribosome reads from our young and aged samples at a given position to the expected ratio based on the total number of reads that map to the transcript. At each position, this allows us to calculate the odds ratio as a measure of enrichment, along with an adjusted p-value to test significance, using the Benjamini-Hochberg correction for multiple hypothesis testing for each gene. The odds ratio is:

$$\text{Odds ratio} = \frac{\frac{Aij}{Yij}}{\frac{\left(\sum_{i=1}^{k} Aij\right) - Aij}{\left(\sum_{i=1}^{k} Yij\right) - Yij}}$$

where A and Y are the ribosomal reads of the aged and young translatome fractions, respectively, at position i of gene j that has length k codons. Age-dependent pause sites

were identified as those that had: (1) Benjamini-Hochberg adjusted p-value < 0.05, (2) 1 < odds ratio < ∞, (3) pause score in the oldest sample greater than the pause score in the intermediate aged sample (Day 6 worms and Day 2 yeast), (4) reads in the oldest sample greater than the average number of reads across the transcript, to control for background, and (5) a position in the internal part of the transcript (i.e. not in the first 20 or last 20 sense codons).

Ribosome occupancy analysis.

Ribosome occupancy for individual genes was plotted using a 5-residue moving average of the pause scores. To analyze ribosome occupancy around polybasic regions, we identified polybasic regions in the genomes of worms and yeast as defined by a stretch of 3, 4, 5, or 6 consecutive residues that were either lysine or arginine (Supplementary Table 3). These regions were categorized into only one group, such that regions of 6 consecutive basic residues was not included in the analysis of the shorter regions. For metagene analysis of ribosome pausing, reads were aligned at the ribosome A-site around the region of interest (e.g. age-dependent pause sites, or the start of the polybasic region). We then calculated the mean and bootstrapped 95% confidence intervals at each position. To control for differences in gene expression and coverage, ribosome reads were normalized by dividing the reads at each codon by the mean number of reads per codon across the analysis window. We excluded low coverage genes that had an average reads per codon across the analysis window less than 0.5.

Pause site sequence analysis.

To examine the enrichment of amino acids and codons associated with greater ribosome pausing during ageing, we first calculated the average frequency of each residue/codon across coding sequences. Using this as background, we generated logo plots to analyze amino acid enrichment in two ways using the R package Logolas[75]. First, we used the tripeptide motifs of age-dependent pause sites in the upper rank of ribosome pausing (pause score > 10 for Day 12 worms, or pause score > 6 for Day 4 yeast). Second, we calculated the average pause score for each of the 8,000 possible tri-peptide motifs across coding sequences and used the motifs that had a higher average pause score, as indicated, and filtered by count (≥ 100) and pause score (average pause score in older sample > 2 in worms and > 1.5 in yeast). We also calculated the residue and codon frequency in the ribosomal active site and compared it to the background frequency within coding sequences.

Other computational analysis.

To examine the association of yeast chronological lifespan with the ability to clear paused, truncated nascent polypeptides, we used previously published datasets[6,62]. We binned yeast strains based on the distribution of the GFP-R12 reporter abundance, as indicated (Fig. 3c). To examine the association of age-dependent ribosome pausing and protein aggregation (Fig. 4e and Extended Data Fig. 10a), we compared our dataset of ribosome pausing to two previous datasets that identified age-dependent protein aggregates in *C. elegans*[37,65]. For the higher coverage dataset[37], we used proteins that were identified in at least three of the four replicates of Day 1 and Day 12 worms, and had an average aggregate abundance at Day 12 higher than that at Day 1. To examine the association of age-dependent ribosome pausing

and ubiquitination (Extended Data Fig. 3e), we compared our dataset of ribosome pausing to a previous dataset examining co-translational ubiquitination in yeast[27].

Immunoblotting.

Yeast strains were grown at 30°C in SC media containing 2% glucose (standard conditions), 3% glycerol, or buffered to pH 6.0 with citrate phosphate buffer (64.2 mM Na_2HPO_4, 17.9 mM citric acid, pH 6.0)[76], as indicated. Day 0 cells were harvested at an OD_{600} of ~0.7, and Day 4 cells were harvested 96 hours later from the same culture. For media swap experiments, overnight cultures were diluted into either fresh SC media or the nutrient-depleted media of the supernatant collected after pelleting Day 4 cells, and Day 0 cells were harvested as above. Frozen cell pellets were resuspended in 200 µl of lysis buffer (50 mM Tris pH 7.5, 150mM NaCl, 1mM EDTA, 5% glycerol, 0.1% Triton X-100, 0.1% SDS, 1mM PMSF, 0.5mM DTT, Roche cOmplete EDTA-free Protease Inhibitor Cocktail), and lysed by vortexing with glass beads at 3000 rpm at 4°C for 3 min, incubating on ice for 3 min, and vortexing again at 3000 rpm at 4°C for 3 min. After clearing by centrifugation of cell lysates at 4,000 rpm at 4°C for 30 sec, protein concentration was normalized by Bradford Assay (Bio-Rad) and 4X NuPage™ LDS Sample Buffer (ThermoFisher) was added. Samples were then boiled for 5 min, run on a 12% SDS-PAGE gel, and transferred to nitrocellulose membrane. Membranes were blocked in 5% milk reconstituted in TBS (20 mM Tris pH 7.5, 150 mL NaCl, 0.1% NaN_3). Primary antibodies were diluted in Antibody Buffer (20 mM Tris pH 7.5, 150 mL NaCl, 0.1% NaN_3, 5% BSA) and secondary antibodies were prepared in 5% milk in TBS. As indicated, blots were subjected to immunblotting using Mouse anti-GFP antibody (Millipore Sigma 11814460001, 1:1000 dilution), Rabbit anti-FLAG antibody (Millipore Sigma F7425, 1:1000 dilution), and Rabbit anti-Histone H3 antibody (EpiCypher 13–0001, 1:2500 dilution), and visualized using the LI-COR system IRDye® 800CW Donkey anti-Mouse IgG (LI-COR 926–32212, 1:10,000 dilution) and IRDye® 680RD Donkey anti-Rabbit IgG (LI-COR 926–68073, 1:10,000 dilution). See Supplementary Data for uncropped immunoblots.

Microscopy.

Yeast cells were grown as above for immunoblotting. Upon harvesting, cells were fixed in 4% paraformaldehyde by incubating at room temperature for 15 min, and washed again in 1X PBS. Cells were then immobilized onto polylysine coated coverslips (Neuvrito) and mounted with ProLong™ Diamond antifade mountant with DAPI (Thermo Fisher). Fluorescence microscopy for quantification was acquired using a Zeiss Axio observer.Z1 inverted microscope equipped with a Plan-Apochromat 100x/1.4 oil DIC M27 objective (Zeiss), X-cite 120 LED system (Lumen Dynamics), filter set (HE) RFP/GFP/DAPI (Zeiss) and a digital Axiocam MRm camera (Zeiss) controlled with the Zen blue software. Raw data was collected as *z*-stacks and projected using ImageJ (NIH), and quantification was performed manually. Confocal microscopy of representative cells was collected on a Leica TCS SP8 inverted sSTED microscope equipped with a 100x/1.40 APO objective and using the following detection mirror settings: RFP 560–630nm, GFP 470–536. DAPI staining was detected using a blue diode 405nm laser (10%) and a photon multiplying tube. One representative middle slide was collected, and images were subsequently deconvolved and background subtracted using Huygens Professional (Scientific Volume Imaging).

Statistical analysis.

All analysis was performed in R (https://www.r-project.org). Gene ontology annotations and significance were obtained using the Database for Annotation, Visualization, and Integrated Discovery (DAVID v6.8)[77] using as background, as indicated, the transcripts included in the Ribo-Seq reference library or present in both this library and the mass spectrometry datasets[37,65]. Statistical significance of categorical variable distributions shown in box plots used two-sided Wilcoxon rank-sum tests (e.g. Fig. 3c). For box plots, the center line represents the median, box limits indicate the upper and lower quartiles, whiskers indicate the 1.5x interquartile range, and points are outliers. Significance of age-dependent puncta formation (Fig. 3b) was assessed using two-sided Welch's *t*-tests. Two-sided Fisher's exact tests were used to calculate significance of residue and codon frequency in age-dependent pause sites (Fig. 2, Fig. 4, Extended Data Fig. 3, and Extended Data Fig. 9), association of ribosome pausing and ubiquitination (Extended Data Fig. 3e), association of ribosome pausing and aggregation (Fig. 4e), and sequence enrichment of protein aggregates (Extended Data Fig. 10b). Additional statistical details are mentioned in the figures or figure legends, including the values of n and P. None of the experiments involved blinding or randomization, and sample size was not predetermined.

Extended Data

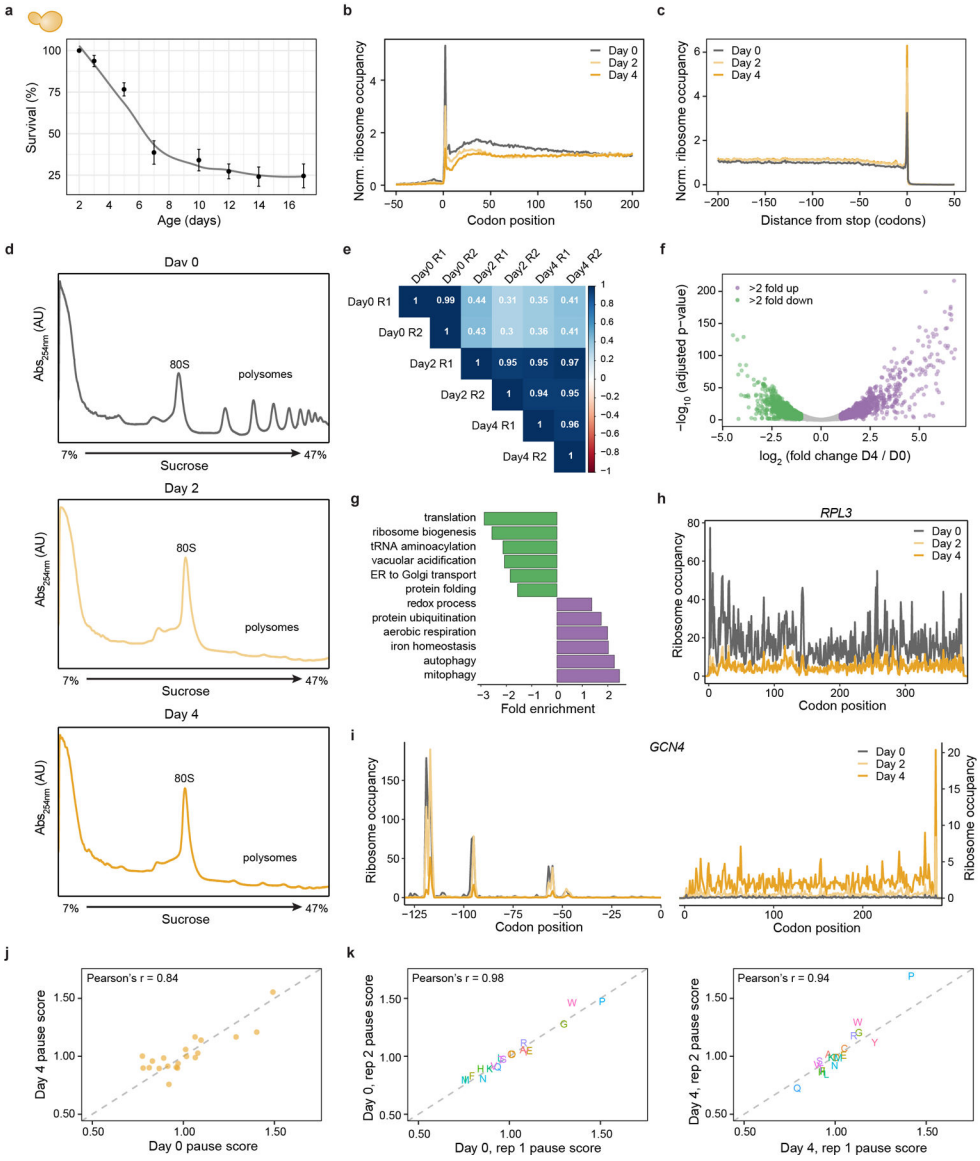

Extended Data Figure 1. Decreased protein synthesis and translatome changes during chronological ageing of yeast.

a, Survival curve of yeast during chronological ageing. $n = 3$ biological replicates with mean ± SEM. **b – c,** Average ribosome occupancy at the **b,** start and **c,** stop codons during yeast chronological ageing. The shaded region represents the 95% bootstrapped confidence interval. **d,** Polysome profiles of chronologically aged yeast at the indicated ages showing decreased population of polysomes during ageing. $n \geq 3$ biological replicates with representative profile shown. **e,** Heat map of gene expression analysis of Ribo-Seq data showing Pearson's correlation coefficient between all yeast samples. **f,** Volcano plot of differential gene expression shows widespread translatome changes for chronologically aged yeast. $n = 2{,}981$ total genes with 901 genes having increased ribosome occupancy (purple, > 2 fold up, adjusted $p < 0.05$, Benjamini-Hochberg method) and 1,033 genes

having decreased ribosome occupancy (green, > 2 fold down, adjusted $p < 0.05$, Benjamini-Hochberg method) in Day 4 yeast cells relative to Day 0 yeast cells. **g,** Functional enrichment of differentially translated genes during ageing displaying representative gene ontology terms (adjusted $p < 0.1$, Benjamini-Hochberg method). See Supplementary Table 2 for complete, unfiltered results. **h,** Ribosome occupancy on ribosomal protein *RPL3* showing decreased translation during yeast ageing. **i,** Ribosome occupancy on the 5'UTR and coding sequence of *GCN4*, showing decreased occupancy at upstream ORFs and increased occupancy across the transcript during ageing. **j,** Scatter plot of average pause score for each amino acid residue in coding sequences of young Day 0 and aged Day 4 yeast. **k,** Scatter plot of average pause score for each amino acid residue in coding sequences of two biological replicates of Day 0 (left) and Day 4 (right) chronologically aged yeast.

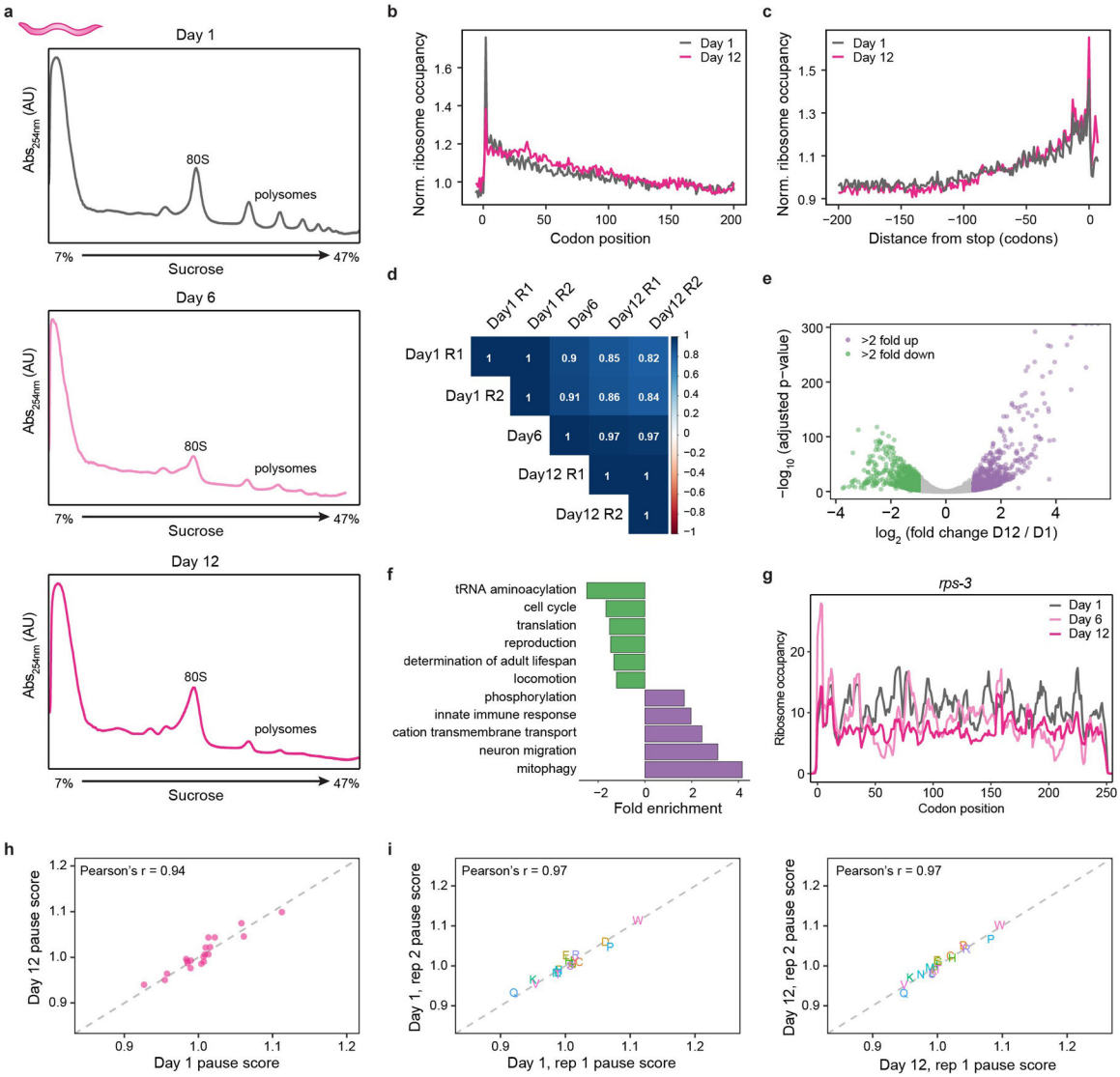

Extended Data Figure 2. Decreased protein synthesis and translatome changes during chronological ageing of worms.

a, Polysome profiles of adult worms at the indicated ages showing decreased population of polysomes during ageing. $n \geq 3$ biological replicates with representative profile shown. **b – c,** Average ribosome occupancy at the **b,** start and **c,** stop codons of young Day 1 and aged Day 12 worms. The shaded region represents the 95% bootstrapped confidence interval. **d,** Heat map of gene expression analysis of Ribo-Seq data showing Pearson's correlation coefficient between worm samples. **e,** Volcano plot of differential gene expression shows widespread translatome changes during worm ageing. $n = 8{,}341$ total genes with 621 genes having increased ribosome occupancy (purple, > 2 fold up, adjusted $p < 0.05$, Benjamini-Hochberg method) and 655 genes having decreased ribosome occupancy (green, > 2 fold down, adjusted $p < 0.05$, Benjamini-Hochberg method) in Day 12 adult worms relative to Day 1 adult worms. **f,** Functional enrichment of differentially translated genes displaying representative gene ontology terms (adjusted $p < 0.1$, except for categories with number of genes < 20 where adjusted $p < 0.25$, Benjamini-Hochberg method). See Supplementary Table 2 for complete, unfiltered results. **g,** Ribosome occupancy on ribosomal protein *rps-3* showing decreased translation during ageing of worms. **h,** Scatter plot of average pause score for each amino acid residue in coding sequences of Day 1 and Day 12 adult worms. **i,** Scatter plot of average pause score for each amino acid residue in coding sequences of two biological replicates of Day 1 (left) and Day 12 (right) adult worms.

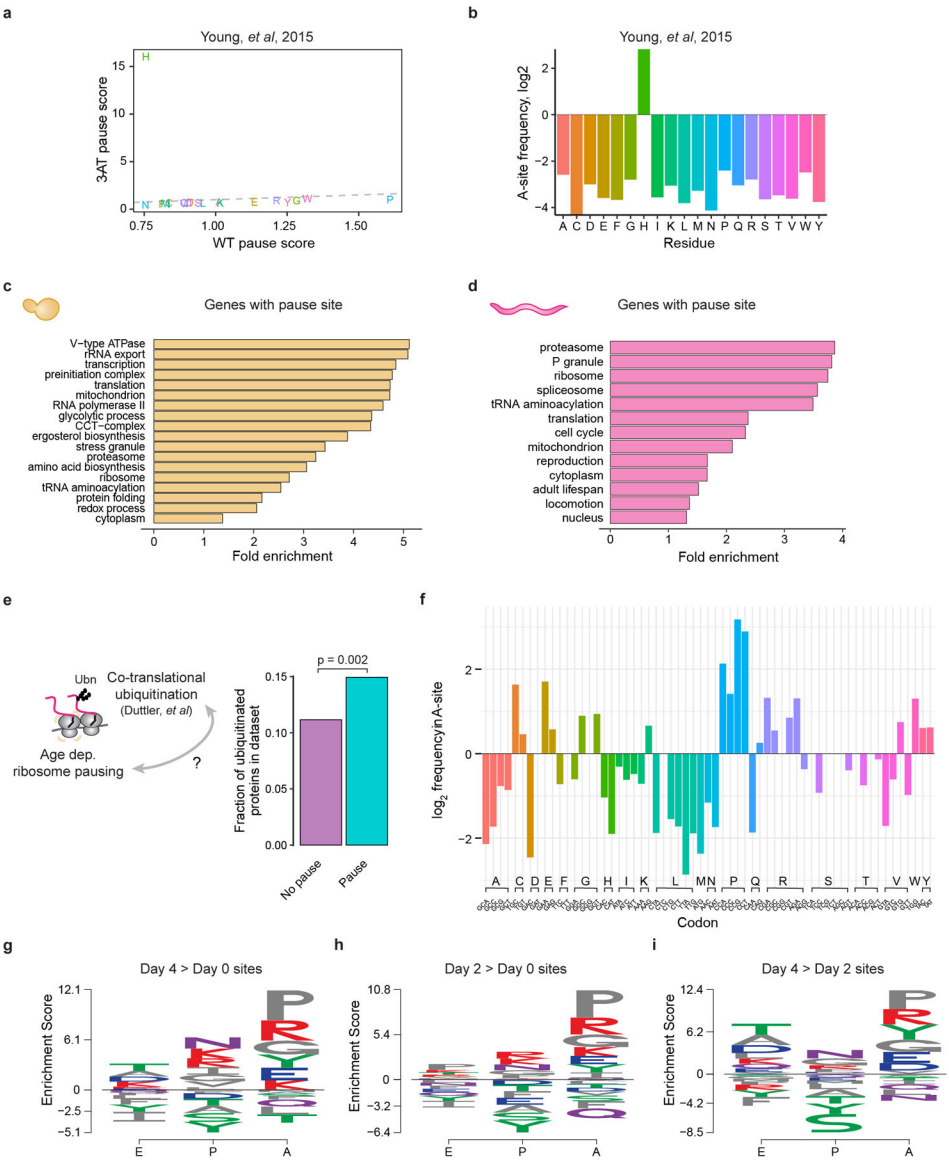

Extended Data Figure 3. Age-dependent ribosome pausing.

a, Scatter plot of the average pause score for each amino acid residue in coding sequences of young WT yeast cells either untreated or treated with 3-amino-1,2,4-triazole (3-AT) from previously published Ribo-Seq data[43]. **b,** Amino acid residue frequency in the ribosomal A-site of statistically significant ribosome pause sites enriched in yeast cells treated with 3-AT[43], relative to the residue frequency in the proteome. **c,** Functional enrichment of genes with an age-dependent pause site in yeast displaying representative gene ontology terms (adjusted $p < 0.1$). See Supplementary Table 2 for complete, unfiltered results. **d,** Functional enrichment of genes with an age-dependent pause site in worms displaying representative gene ontology terms (adjusted $p < 0.1$). See Supplementary Table 2 for complete, unfiltered results. **e,** Investigating the association between age-dependent ribosome pausing and co-translational ubiquitination[27]. Population $n = 937$ transcripts with a pause site, 3,145 transcripts without a pause site. $p = 0.002$, two-sided Fisher's exact test. **f,** Codon frequency

in the ribosomal A-site of age-dependent ribosome pause sites relative to the codon frequency in the genome. n = 271 pause sites with Day 4 pause score > 6 in 232 genes. **g – i,** Peptide motif associated with greater ribosome pausing in the indicated age comparisons.

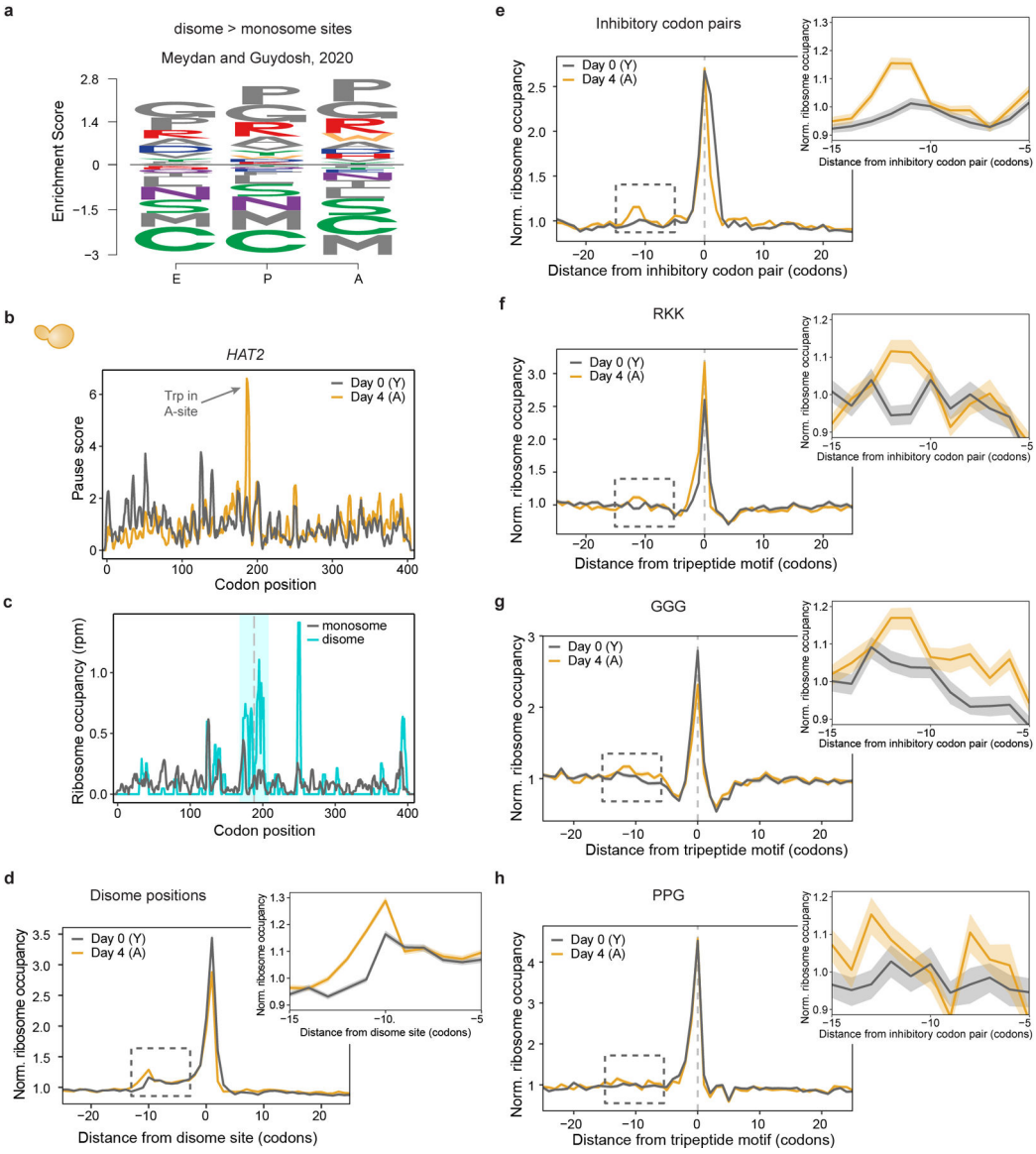

Extended Data Figure 4. Association of age-dependent ribosome pausing in yeast with disome formation.

a, Peptide motif associated with disome formation in young cells[47]. **b,** Ribosome occupancy on *HAT2* with ribosome pausing at position 188 with Trp in the A-site. **c,** Occupancy of monosomes and disomes on *HAT2* from disome footprint profiling of young cells[47]. **d – h,** Average ribosome occupancy in young and aged yeast, with a lagging ribosome peak present in aged cells, at **d,** the position where disomes were most enriched in each transcript in young cells[47]; **e,** inhibitory codon pairs previously associated with ribosome pausing[48] and disome formation[47]; and **f – h,** tripeptide motifs previously associated with disome formation[47]. The shaded region represents the 95% bootstrapped confidence interval.

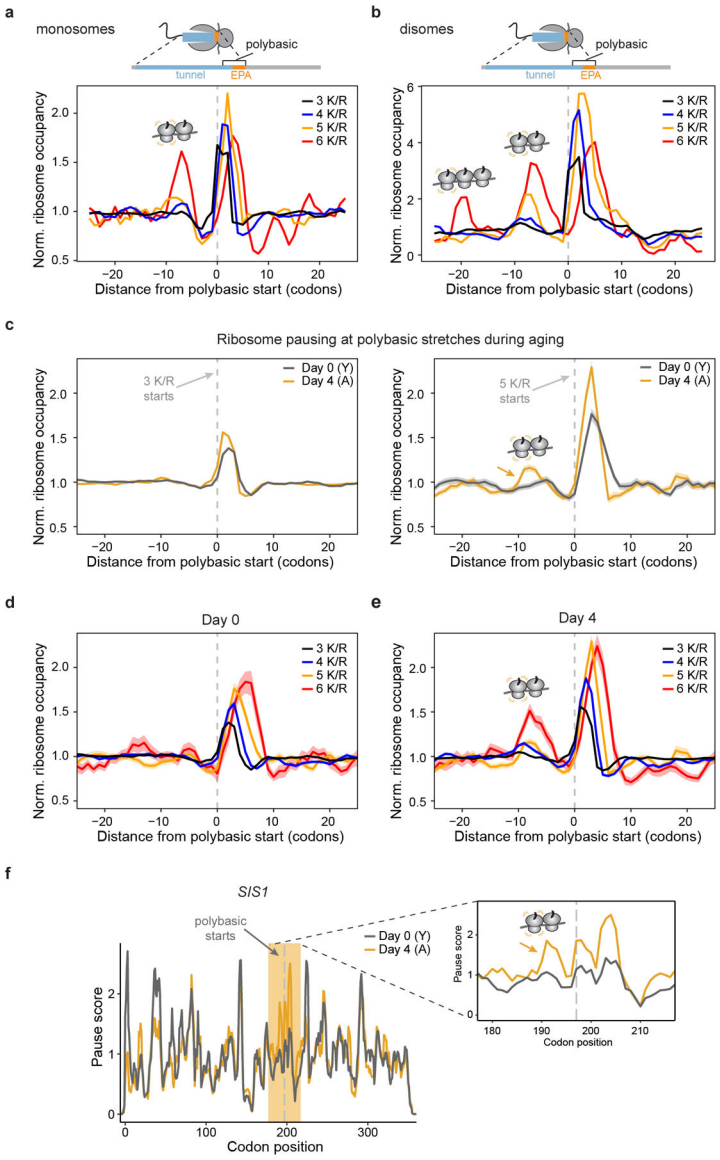

Extended Data Figure 5. Age-dependent ribosome pausing at polybasic regions.

a – b, Average ribosome occupancy at polybasic regions of **a,** monosomes and **b,** disomes in young WT yeast[47] showing length-dependent pausing and collisions. **c,** Average ribosome occupancy at polybasic regions consisting of 3 (left) or 5 (right) consecutive Lys or Arg (K/R) for young Day 0 and aged Day 4 yeast. n = 3,729 sites of 3 K/R in 2,198 genes, and 159 sites of 5 K/R in 152 genes. The shaded region represents the 95% bootstrapped confidence interval. Arrow indicates a putative increase in ribosome collision events with age at regions with 5 K/R. **d – e,** Average ribosome occupancy at polybasic regions of **d,** young Day 0 and **e,** aged Day 4 yeast. Also see panel c and Figure 2c and 2d. **f,** Ribosome occupancy on *SIS1* with inset highlighting ribosome pausing and collision (arrow) at stretch of 6 K/R within a 10 residue window.

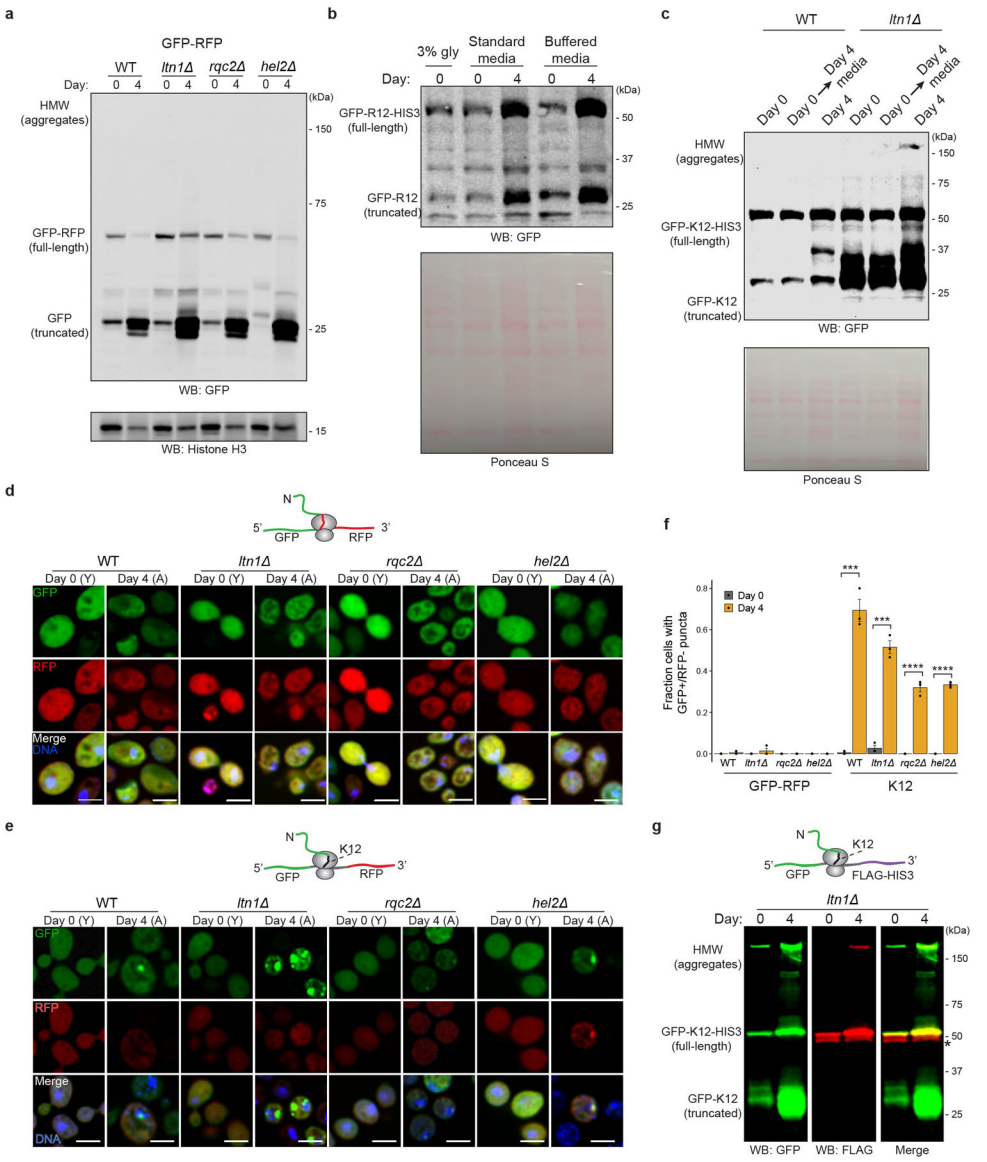

Extended Data Figure 6. Age-dependent aberrant translation and aggregation of truncated nascent polypeptides in yeast.

a, Immunoblot of young Day 0 and aged Day 4 yeast of the indicated strain harboring the no-insert *GFP-RFP* control reporter. Truncated and full-length products are noted. $n \geq 3$ biological replicates with representative example shown. For gel source data, see Supplementary Figure 1. **b,** Increased formation of truncated polypeptides in chronologically aged yeast is not due to acidification of the media or respiratory conditions. Immunoblot of young Day 0 and aged Day 4 WT yeast harboring the *GFP-R12-FLAG-HIS3* ribosome pausing reporter and grown in standard media containing 2% glucose as carbon source, media buffered to pH 6.0, or media containing 3% glycerol. $n \geq 3$ biological replicates with representative example shown. For gel source data, see Supplementary Figure 2. **c,** Depletion of media nutrients during yeast chronological ageing does not increase formation of truncated polypeptides. Immunoblot of *GFP-K12-FLAG-HIS3* ribosome pausing reporter from young Day 0 and aged Day 4 WT or *ltn1Δ* yeast, as well as after

swapping media (i.e. young Day 0 yeast cells grown in “aged” media from Day 4 cells). $n \geq 3$ biological replicates with representative example shown. For gel source data, see Supplementary Figure 2. **d – f,** Fluorescence microscopy examining puncta formation in young (Y) Day 0 and aged (A) Day 4 yeast of WT and RQC mutant cells harboring **d,** GFP-RFP, or **e,** the ribosome pausing reporter with 12 K inserted between *GFP* and *RFP*. $n \geq 3$ biological replicates with representative example shown. Scale bar: 3 μm. **f,** Associated quantification of GFP+/RFP- puncta from $n \geq 200$ cells from 3 biological replicates with mean ± SEM. For cells harboring the K12 reporter: WT: $p = 2.2e^{-4}$, *ltn1Δ*: $p = 1.3e^{-4}$; *rqc2Δ*: $p = 9.6e^{-5}$, *hel2Δ*: $p = 1.7e^{-6}$, two-sided Welch’s *t*-test. **g,** Immunoblot of young Day 0 and aged Day 4 *ltn1Δ* yeast harboring the *GFP-K12-FLAG-HIS3* ribosome pausing reporter and probed with αGFP and αFLAG antibodies. Truncated, full-length, and high-molecular weight (HMW) species are noted. $n \geq 3$ biological replicates with representative example shown. An asterisk around 50 kDa indicates a non-specific band from αFLAG antibody. For gel source data, see Supplementary Figure 2.

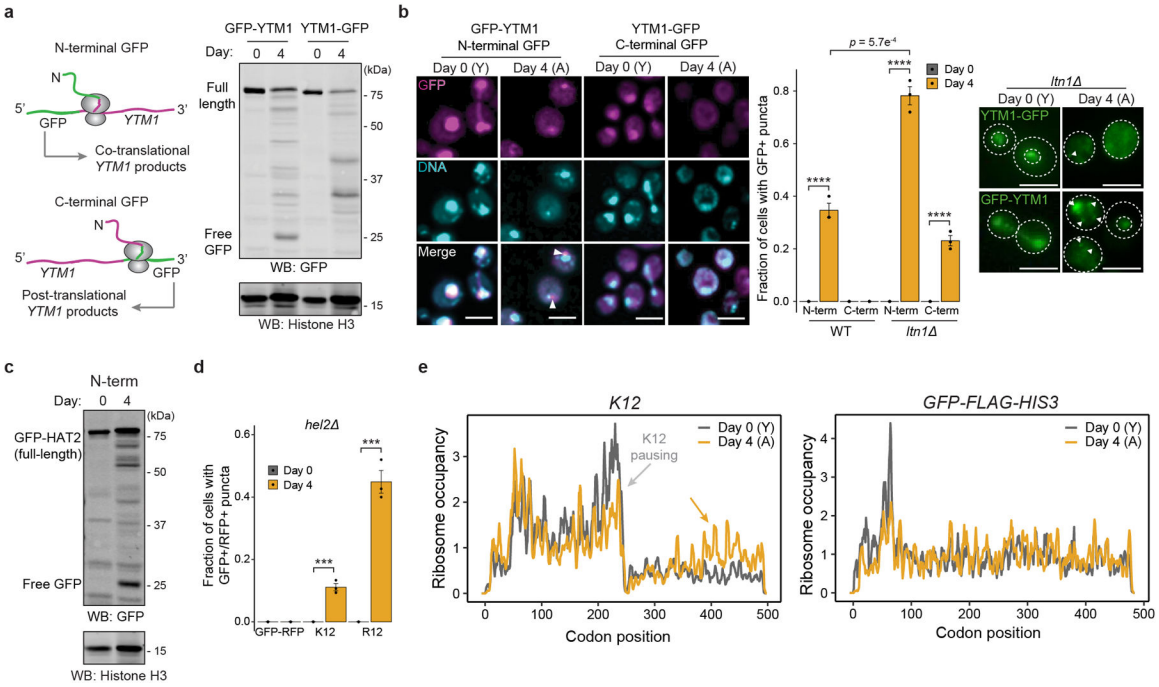

Extended Data Figure 7. Age-dependent ribosome pausing, aberrant translation, and aggregation of endogenous yeast proteins and reporters.

a, Immunoblot of young Day 0 and aged Day 4 yeast harboring GFP-tagged *YTM1* that is either N-terminally tagged to monitor co-translational products or C-terminally tagged to monitor post-translational degradation products. $n = 3$ biological replicates with representative example shown. For gel source data, see Supplementary Figure 3. **b,** Fluorescence microscopy and quantification of GFP+ puncta of GFP-tagged *YTM1* in young and aged WT and *ltn1Δ* yeast cells. $n \geq 200$ cells from 3 biological replicates with mean ± SEM; WT N-term: $p = 2.0e^{-4}$; *ltn1Δ* N-term: $p = 2.3e^{-5}$; *ltn1Δ* C-term: $p = 2.8e^{-4}$, two-sided Welch’s *t*-test. Scale bar: 3 μm. **c,** Immunoblot of young Day 0 and aged Day 4 yeast harboring N-terminally GFP-tagged *HAT2* showing increased truncated co-

translational products during ageing. $n = 3$ biological replicates with representative example shown. For gel source data, see Supplementary Figure 3. **d,** Quantification of GFP+/RFP+ puncta in *hel2Δ* cells using the indicated reporter. $n \geq 200$ cells from 3 biological replicates with mean ± SEM; K12: $p = 7.0e^{-4}$; R12: $p = 2.5e^{-4}$, two-sided Welch's *t*-test. **e,** Ribosome occupancy across the stalling reporter *GFP-K12-FLAG-HIS3* (left) and the no-insert control (right) of young Day 0 and aged Day 4 yeast, showing increased occupancy in 3' end of the stalling reporter transcript during ageing.

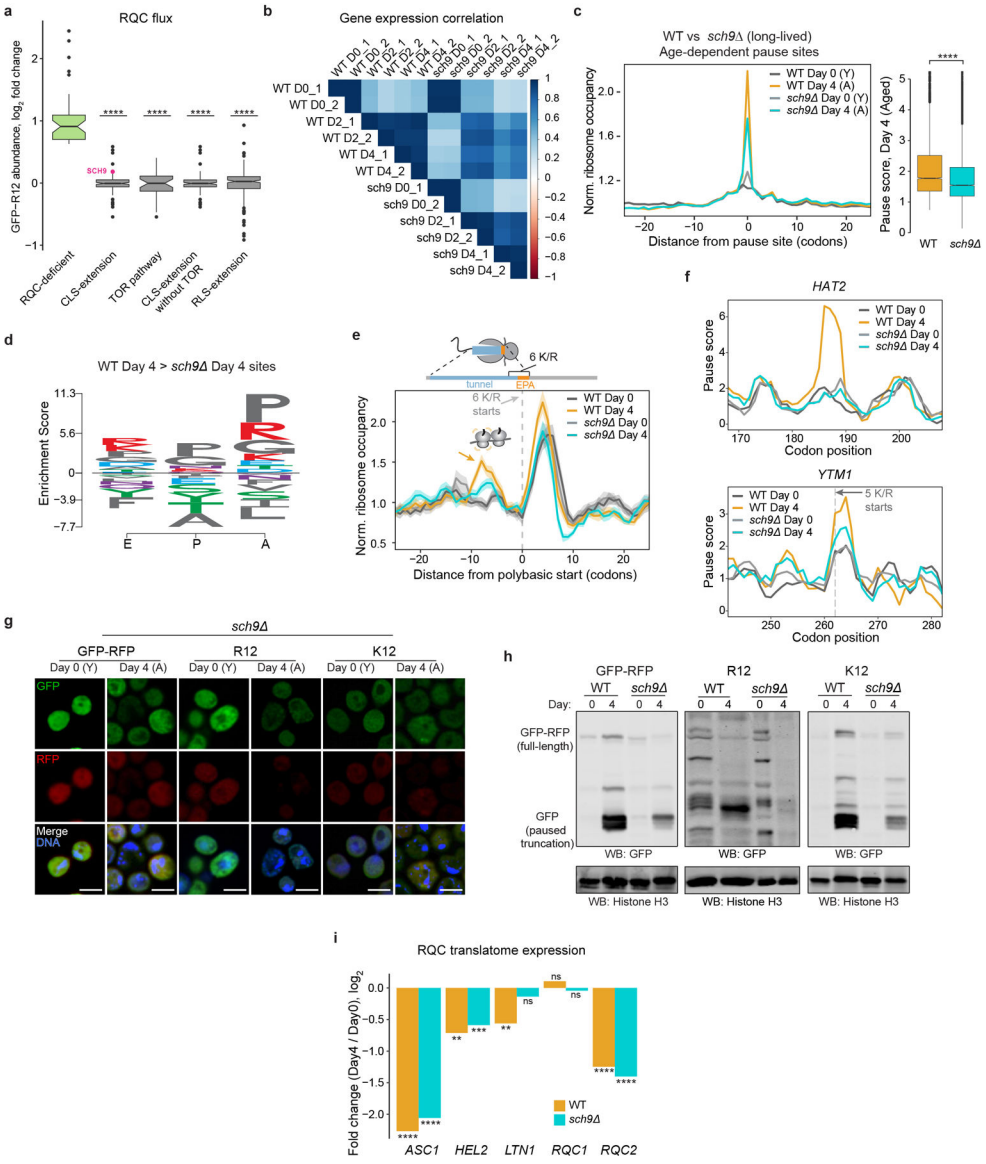

Extended Data Figure 8. Association of extended lifespan with improved RQC flux and reduced ribosome pausing and collision.

a, RQC flux was assessed based on the abundance of the *GFP-R12-HIS3* ribosome pausing reporter[6]. RQC flux of the following four groups of genes was compared to yeast strains with deficient RQC (i.e. strains with reporter GFP abundance greater than 3 standard deviations above the mean of the total collection[6]; $n = 39$): 1) long-lived CLS strains

(strains with a chronological lifespan greater than 1 standard deviation above the mean of the total collection[62]; $n = 150$, $p = 7.3e^{-22}$, two-sided Wilcoxon rank-sum test), 2) genes involved in the TOR pathway ($n = 31$, $p = 2.8e^{-20}$, two-sided Wilcoxon rank-sum test), 3) long-lived CLS strains not involved in the TOR pathway ($n = 142$, $p = 9.3e^{-23}$, two-sided Wilcoxon rank-sum test), and 4) long-lived RLS strains[78] ($n = 201$, $p = 1.3e^{-21}$, two-sided Wilcoxon rank-sum test). **b,** Heat map of gene expression analysis of Ribo-Seq data showing Pearson's correlation coefficient between all yeast samples. **c,** Average ribosome occupancy at age-dependent pause sites ($n = 5{,}951$ sites in 937 genes) in the indicated strains, with the distribution of pause scores in aged (A) Day 4 WT and *sch9Δ* yeast cells on the right ($p = 2.5e^{-77}$, two-sided Wilcoxon rank-sum test). **d,** Peptide motif associated with positions in the translatome where ribosome pausing is greater in aged Day 4 WT yeast relative to aged Day 4 *sch9Δ* yeast. **e,** Average ribosome occupancy in WT and *sch9Δ* yeast at polybasic regions consisting of 6 consecutive Lys or Arg (K/R). $n = 60$ K/R sites in 58 genes. The shaded region represents the 95% bootstrapped confidence interval. Arrow indicates a putative increase in ribosome collision events. **f,** Ribosome occupancy on *HAT2* (top) and *YTM1* (bottom) in the indicated yeast strains around age-dependent ribosome pause sites (*HAT2*: position 188 with Trp in the A-site; *YTM1*: a stretch of 5 consecutive K/R). **g,** Fluorescence microscopy of GFP+/RFP- puncta formation in young (Y) Day 0 and aged (A) Day 4 yeast of WT and *sch9Δ* cells harboring the indicated reporter. $n \geq 3$ biological replicates with representative example shown. Scale bar: 3 um. **h,** Immunoblot of young Day 0 and aged Day 4 yeast of WT or *sch9Δ* cells harboring the indicated reporter. Truncated and full-length products are noted. $n \geq 3$ biological replicates with representative example shown. For gel source data, see Supplementary Figure 4. **i,** Relative gene expression of RQC machinery in the translatome of WT or *sch9Δ* cells comparing aged Day 4 yeast to young Day 0 yeast. ns = not significant; WT / *sch9Δ* cells: *ASC1*: $p = 4.1e^{-40}$ / $9.8e^{-26}$, *HEL2*: $p = 0.002$ / $1.3e^{-4}$, *LTN1*: $p = 0.006$ / ns, *RQC2*: $p = 1.2e^{-9}$ / $2.0e^{-20}$, two-sided Wald test with Benjamini-Hochberg correction.

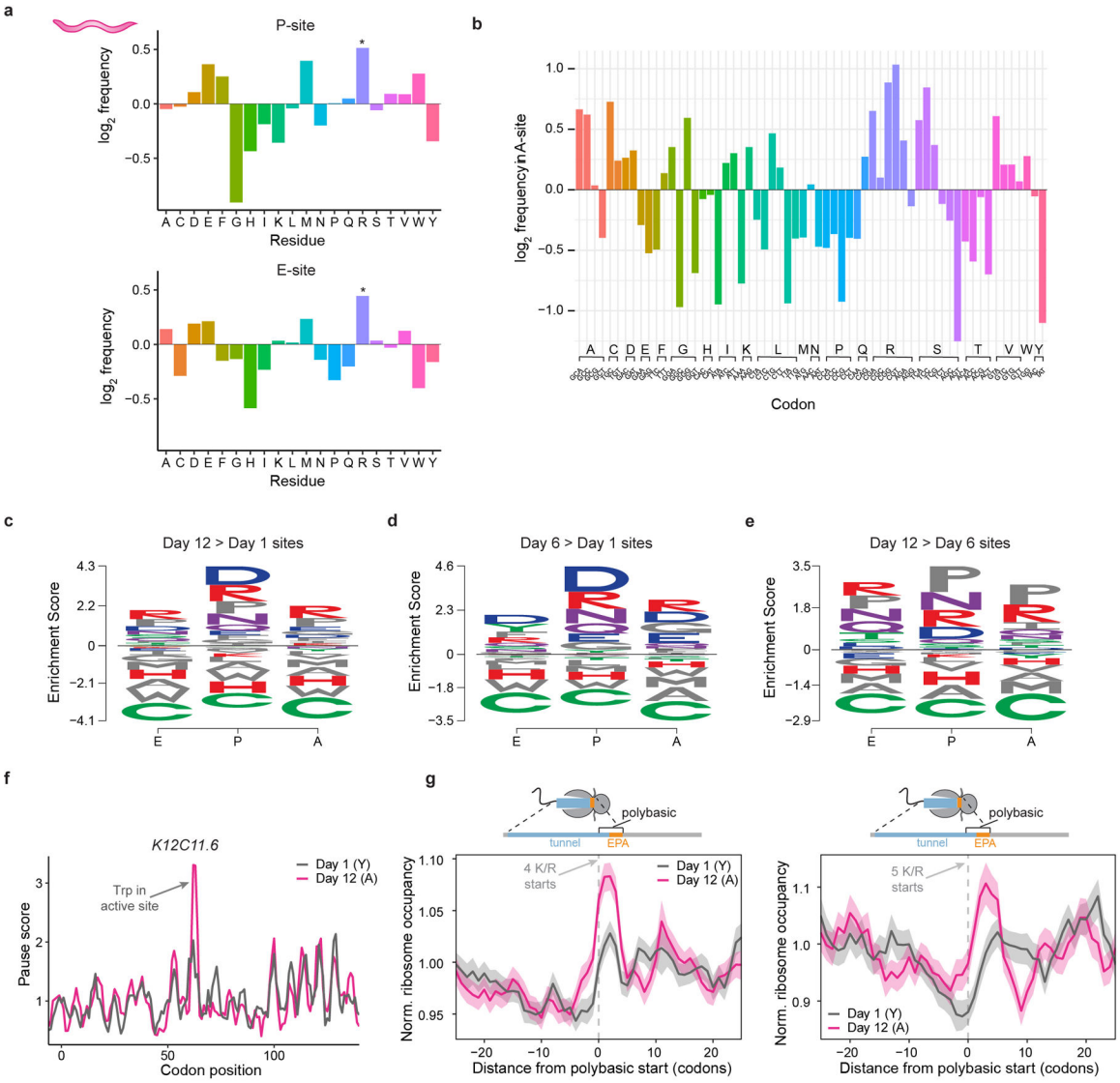

Extended Data Figure 9. Sequence specificity of age-dependent ribosome pausing in worms.

a, Amino acid residue frequency in the ribosomal P- and E-sites of age-dependent ribosome pause sites relative to the residue frequency in the proteome. $n = 587$ pause sites with Day 12 pause score > 10 in 437 genes. P-site Arg: $p = 0.01$, E-site Arg: $p = 0.04$, two-sided Fisher's exact test. **b,** Codon frequency in the ribosomal A-site of age-dependent ribosome pause sites relative to the codon frequency in the genome. $n = 587$ pause sites with Day 12 pause score > 10 in 437 genes. **c – e,** Peptide motif associated with greater ribosome pausing in the indicated age comparisons. **f,** Ribosome occupancy on *K12C11.6* with ribosome pausing at position 62 with Trp in the ribosomal active site. **g,** Average ribosome occupancy at polybasic regions consisting of 4 (left) or 5 (right) consecutive Lys or Arg (K/R). $n =$ 1,396 sites of 4 K/R in 1,720 genes, and 369 sites of 5 K/R in 348 genes. The shaded region represents the 95% bootstrapped confidence interval.

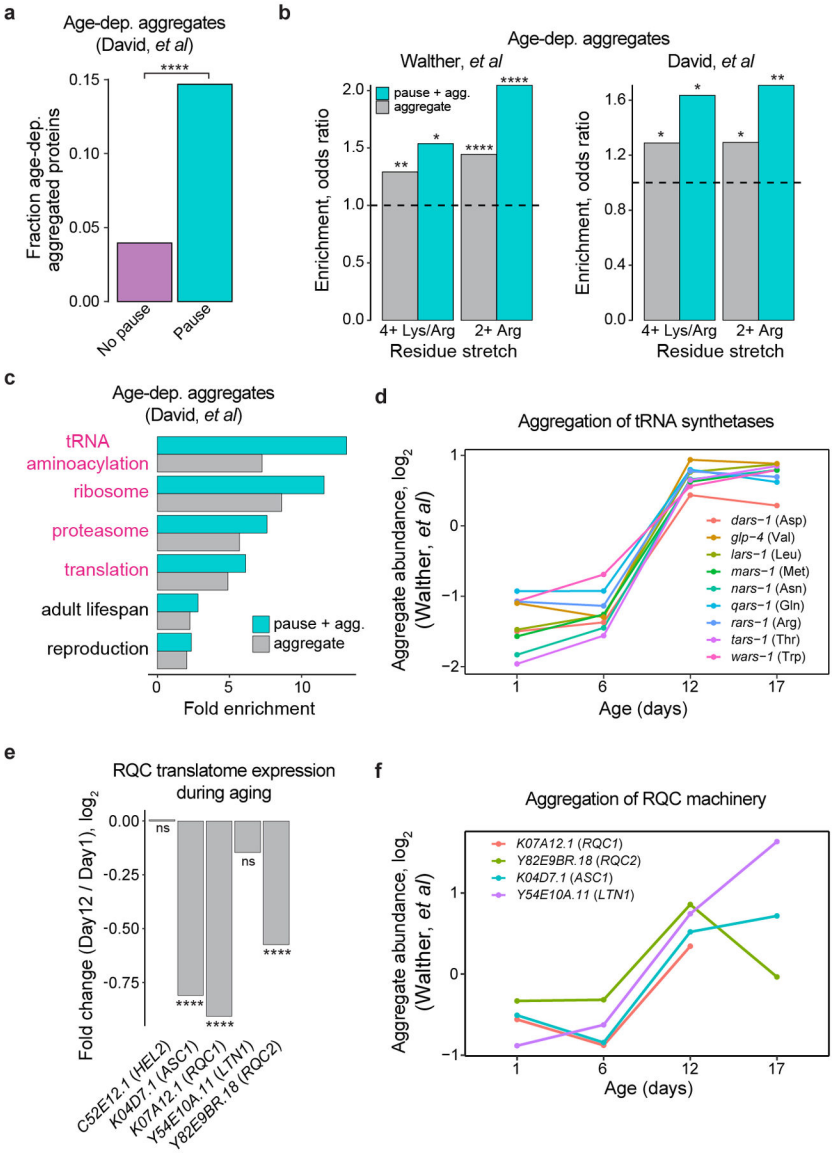

Extended Data Figure 10. Association of age-dependent aggregation and ribosome pausing in worms.

a, Investigating the association between age-dependent ribosome pausing and aggregation[65]. Population $n = 742$ proteins with pause site, 6,219 proteins without a pause site. $p = 1.6e^{-23}$, two-sided Fisher's exact test. **b,** Enrichment of polybasic regions (4 or more consecutive Lys or Arg, and 2 or more consecutive Arg) in age-dependent aggregated proteins from two different datasets[37,65], and those proteins that also have age-dependent ribosome pausing. Walther, *et al*: 4+ Lys/Arg: aggregate / pause + agg.: $p = 0.01$ / 0.03, 2+ Arg: aggregate / pause + agg.: $p = 4.9e^{-6}$ / $4.8e^{-5}$; David, *et al*: 4+ Lys/Arg: aggregate / pause + agg.: $p = 0.05$ / 0.04, 2+ Arg: aggregate / pause + agg.: $p = 0.02$ / 0.01, two-sided Fisher's exact test. **c,** Comparing the functional enrichment within aggregated proteins[65] to those that also have age-dependent ribosome pausing, displaying representative gene ontology terms (adjusted $p < 0.05$, Benjamini-Hochberg correction). Categories related to proteostasis are highlighted. Also see Supplementary Table 2. **d,** Aggregate abundance[37] over time of tRNA

synthetases exhibiting both age-dependent aggregation and ribosome pausing. **e,** Relative gene expression of worm RQC orthologs (yeast ortholog in parentheses) in the translatome in aged Day 12 adult worms compared to young Day 1 worms. ns = not significant, *K04D7.1*: $p = 1.2e^{-14}$, *K07A12.1*: $p = 3.9e^{-18}$, *Y82E9BR.18*: $p = 5.4e^{-7}$, two-sided Wald test with Benjamini-Hochberg correction. **f,** Aggregate abundance[37] over time of worm RQC orthologs.

Supplementary Material

Refer to Web version on PubMed Central for supplementary material.

Acknowledgements

We thank R. Aviner and M. Aguilar-Rangel for comments on the manuscript, the Frydman Laboratory for discussions and advice, J. Chartron, P. Dolan, and K. Dalton for technical input, and J. Lim and J. Arribere for *C. elegans* expertise. *YTM1* and *HAT2* N-terminally GFP tagged seamless yeast strains were generous gifts from D. Jarosz, and Rabbit anti-Histone H3 antibody was a generous gift from R. Farr and O. Gozani. Sequencing was performed at the UCSF Center for Advanced Technology. K.C.S. was supported as a Glenn Foundation for Medical Research Postdoctoral Fellow and by NIH/NIA grant T32AG047126. F.M-P. was supported by The Pew Trusts in the Biomedical Sciences postdoctoral Award (00034104), and T.K.R was supported by NIH/NIGMS National Research Service Award (F32GM120947). This work was supported by NIH grants GM056433 and AG054407 (J.F.). JF is a CZ Biohub Investigator.

Data availability

The datasets generated for this study are deposited in NCBI's Gene Expression Omnibus (GEO) under GEO Series accession number GSE152850. Additional datasets used in this study are also publicly available: GSE139036 (disome profiling), GSE69414 and GSE52968 (Ribo-Seq of yeast treated with 3-AT), doi: 10.1101/gad.1381406 (yeast chronological lifespan), doi: 10.1016/j.cell.2012.10.044 (RQC flux), doi: 10.1016/j.cell.2015.03.032 and doi: 10.1371/journal.pbio.1000450 (protein aggregation during *C. elegans* aging).

References

1. López-Otín C, Blasco MA, Partridge L, Serrano M & Kroemer G The hallmarks of aging. Cell 153, 1194–1217 (2013). [PubMed: 23746838]
2. Chiti F & Dobson CM Protein misfolding, functional amyloid, and human disease. Annu Rev Biochem 75, 333–366 (2006). [PubMed: 16756495]
3. Pechmann S, Willmund F & Frydman J The ribosome as a hub for protein quality control. Mol Cell 49, 411–421 (2013). [PubMed: 23395271]
4. Simms CL, Yan LL & Zaher HS Ribosome Collision Is Critical for Quality Control during No-Go Decay. Mol Cell 68, 1–19 (2017). [PubMed: 28985500]
5. Juszkiewicz S et al. ZNF598 Is a Quality Control Sensor of Collided Ribosomes. Mol Cell 1–21 (2018). doi:10.1016/j.molcel.2018.08.037
6. Brandman O et al. A ribosome-bound quality control complex triggers degradation of nascent peptides and signals translation stress. Cell 151, 1042–1054 (2012). [PubMed: 23178123]
7. Balchin D, Hayer-Hartl M & Hartl FU In vivo aspects of protein folding and quality control. Science 353, aac4354–aac4354 (2016). [PubMed: 27365453]
8. Jahn TR & Radford SE Folding versus aggregation: polypeptide conformations on competing pathways. 469, 100–117 (2008).

9. Ciryam P, Tartaglia GG, Morimoto RI, Dobson CM & Vendruscolo M Widespread aggregation and neurodegenerative diseases are associated with supersaturated proteins. CellReports 5, 781–790 (2013).
10. Gingold H & Pilpel Y Determinants of translation efficiency and accuracy. Mol Syst Biol 7, 481 (2011). [PubMed: 21487400]
11. Stein KC & Frydman J The stop-and-go traffic regulating protein biogenesis: How translation kinetics controls proteostasis. J Biol Chem 294, 2076–2084 (2019). [PubMed: 30504455]
12. Yu C-H et al. Codon Usage Influences the Local Rate of Translation Elongation to Regulate Co-translational Protein Folding. Mol Cell 59, 744–754 (2015). [PubMed: 26321254]
13. Pechmann S & Frydman J Evolutionary conservation of codon optimality reveals hidden signatures of cotranslational folding. Nat Struct Mol Biol 20, 237–243 (2013). [PubMed: 23262490]
14. Kudla G, Murray AW, Tollervey D & Plotkin JB Coding-sequence determinants of gene expression in Escherichia coli. Science 324, 255–258 (2009). [PubMed: 19359587]
15. Zhang G, Hubalewska M & Ignatova Z Transient ribosomal attenuation coordinates protein synthesis and co-translational folding. Nat Struct Mol Biol 16, 274–280 (2009). [PubMed: 19198590]
16. Collart MA & Weiss B Ribosome pausing, a dangerous necessity for co-translational events. Nucleic Acids Res 48, 1043–1055 (2020). [PubMed: 31598688]
17. Chartron JW, Hunt KCL & Frydman J Cotranslational signal-independent SRP preloading during membrane targeting. 536, 1–15 (2016).
18. Pechmann S, Chartron JW & Frydman J Local slowdown of translation by nonoptimal codons promotes nascent-chain recognition by SRP in vivo. Nat Struct Mol Biol 21, 1100–1105 (2014). [PubMed: 25420103]
19. Stein KC, Kriel A & Frydman J Nascent Polypeptide Domain Topology and Elongation Rate Direct the Cotranslational Hierarchy of Hsp70 and TRiC/CCT. Mol Cell 75, 1117–1130.e5 (2019). [PubMed: 31400849]
20. Sitron CS & Brandman O Detection and Degradation of Stalled Nascent Chains via Ribosome-Associated Quality Control. Annu Rev Biochem 89, 417–442 (2020). [PubMed: 32569528]
21. Brandman O & Hegde RS Ribosome-associated protein quality control. Nat Struct Mol Biol 23, 7–15 (2016). [PubMed: 26733220]
22. Dimitrova LN, Kuroha K, Tatematsu T & Inada T Nascent peptide-dependent translation arrest leads to Not4p-mediated protein degradation by the proteasome. J Biol Chem 284, 10343–10352 (2009). [PubMed: 19204001]
23. Buhr F et al. Synonymous Codons Direct Cotranslational Folding toward Different Protein Conformations. Mol Cell 61, 341–351 (2016). [PubMed: 26849192]
24. Nedialkova DD & Leidel SA Optimization of Codon Translation Rates via tRNA Modifications Maintains Proteome Integrity. Cell 161, 1606–1618 (2015). [PubMed: 26052047]
25. Kim SJ et al. Protein folding. Translational tuning optimizes nascent protein folding in cells. Science 348, 444–448 (2015). [PubMed: 25908822]
26. Willmund F et al. The cotranslational function of ribosome-associated Hsp70 in eukaryotic protein homeostasis. Cell 152, 196–209 (2013). [PubMed: 23332755]
27. Duttler S, Pechmann S & Frydman J Principles of cotranslational ubiquitination and quality control at the ribosome. Mol Cell 50, 379–393 (2013). [PubMed: 23583075]
28. Koplin A et al. A dual function for chaperones SSB-RAC and the NAC nascent polypeptide-associated complex on ribosomes. 189, 57–68 (2010).
29. Choe Y-J et al. Failure of RQC machinery causes protein aggregation and proteotoxic stress. 531, 191–195 (2016).
30. Yonashiro R et al. The Rqc2/Tae2 subunit of the ribosome-associated quality control (RQC) complex marks ribosome-stalled nascent polypeptide chains for aggregation. eLife 5, 146 (2016).
31. Wu CC-C, Peterson A, Zinshteyn B, Regot S & Green R Ribosome Collisions Trigger General Stress Responses to Regulate Cell Fate. Cell (2020). doi:10.1016/j.cell.2020.06.006
32. Ishimura R et al. RNA function. Ribosome stalling induced by mutation of a CNS-specific tRNA causes neurodegeneration. Science 345, 455–459 (2014). [PubMed: 25061210]

33. Bengtson MH & Joazeiro CAP Role of a ribosome-associated E3 ubiquitin ligase in protein quality control. 467, 470–473 (2010).
34. Taylor RC & Dillin A Aging as an event of proteostasis collapse. Cold Spring Harbor Perspectives in Biology 3, (2011).
35. Ben-Zvi A, Miller EA & Morimoto RI Collapse of proteostasis represents an early molecular event in Caenorhabditis elegans aging. Proc Natl Acad Sci USA 106, 14914–14919 (2009). [PubMed: 19706382]
36. Steffen KK & Dillin A A Ribosomal Perspective on Proteostasis and Aging. Cell Metabolism 23, 1004–1012 (2016). [PubMed: 27304502]
37. Walther DM et al. Widespread Proteome Remodeling and Aggregation in Aging C. elegans. Cell 161, 919–932 (2015). [PubMed: 25957690]
38. Pan KZ et al. Inhibition of mRNA translation extends lifespan in Caenorhabditis elegans. Aging Cell 6, 111–119 (2007). [PubMed: 17266680]
39. Hansen M et al. Lifespan extension by conditions that inhibit translation in Caenorhabditis elegans. Aging Cell 6, 95–110 (2007). [PubMed: 17266679]
40. Reis-Rodrigues P et al. Proteomic analysis of age-dependent changes in protein solubility identifies genes that modulate lifespan. Aging Cell 11, 120–127 (2012). [PubMed: 22103665]
41. Narayan V et al. Deep Proteome Analysis Identifies Age-Related Processes in C. elegans. Cell Systems 3, 144–159 (2016). [PubMed: 27453442]
42. Hu Z et al. Ssd1 and Gcn2 suppress global translation efficiency in replicatively aged yeast while their activation extends lifespan. eLife 7, 4443 (2018).
43. Young DJ, Guydosh NR, Zhang F, Hinnebusch AG & Green R Rli1/ABCE1 Recycles Terminating Ribosomes and Controls Translation Reinitiation in 3'UTRs In Vivo. Cell 162, 872–884 (2015). [PubMed: 26276635]
44. Guydosh NR & Green R Dom34 rescues ribosomes in 3' untranslated regions. Cell 156, 950–962 (2014). [PubMed: 24581494]
45. Choi J et al. How Messenger RNA and Nascent Chain Sequences Regulate Translation Elongation. Annu Rev Biochem 87, 421–449 (2018). [PubMed: 29925264]
46. Schuller AP, Wu CC-C, Dever TE, Buskirk AR & Green R eIF5A Functions Globally in Translation Elongation and Termination. Mol Cell 66, 1–30 (2017). [PubMed: 28388436]
47. Meydan S & Guydosh NR Disome and Trisome Profiling Reveal Genome-wide Targets of Ribosome Quality Control. Mol Cell 79, 588–602.e6 (2020). [PubMed: 32615089]
48. Gamble CE, Brule CE, Dean KM, Fields S & Grayhack EJ Adjacent Codons Act in Concert to Modulate Translation Efficiency in Yeast. Cell 166, 679–690 (2016). [PubMed: 27374328]
49. Han P et al. Genome-wide Survey of Ribosome Collision. CellReports 31, 107610 (2020).
50. Juszkiewicz S, Speldewinde SH, Wan L, Svejstrup JQ & Hegde RS The ASC-1 Complex Disassembles Collided Ribosomes. Mol Cell (2020). doi:10.1016/j.molcel.2020.06.006
51. Ikeuchi K et al. Collided ribosomes form a unique structural interface to induce Hel2-driven quality control pathways. EMBO J 38, (2019).
52. Shen PS et al. Protein synthesis. Rqc2p and 60S ribosomal subunits mediate mRNA-independent elongation of nascent chains. Science 347, 75–78 (2015). [PubMed: 25554787]
53. Shao S, Malsburg von der, K. & Hegde RS Listerin-Dependent Nascent Protein Ubiquitination Relies on Ribosome Subunit Dissociation. Mol Cell 50, 637–648 (2013). [PubMed: 23685075]
54. Shao S & Hegde RS Reconstitution of a minimal ribosome-associated ubiquitination pathway with purified factors. Mol Cell 55, 880–890 (2014). [PubMed: 25132172]
55. Shao S, Brown A, Santhanam B & Hegde RS Structure and assembly pathway of the ribosome quality control complex. Mol Cell 57, 433–444 (2015). [PubMed: 25578875]
56. Juszkiewicz S & Hegde RS Initiation of Quality Control during Poly(A) Translation Requires Site-Specific Ribosome Ubiquitination. Mol Cell 65, 743–750.e4 (2017). [PubMed: 28065601]
57. Sundaramoorthy E et al. ZNF598 and RACK1 Regulate Mammalian Ribosome-Associated Quality Control Function by Mediating Regulatory 40S Ribosomal Ubiquitylation. Mol Cell 65, 751–760.e4 (2017). [PubMed: 28132843]

58. Matsuo Y et al. Ubiquitination of stalled ribosome triggers ribosome-associated quality control. Nature communications 8, 1–13 (2017).
59. Tsuboi T et al. Dom34:hbs1 plays a general role in quality-control systems by dissociation of a stalled ribosome at the 3' end of aberrant mRNA. Mol Cell 46, 518–529 (2012). [PubMed: 22503425]
60. Sitron CS & Brandman O CAT tails drive on- and off-ribosome degradation of stalled polypeptides. 1–29 (2018). doi:10.1101/469296
61. Anisimova AS et al. Multifaceted deregulation of gene expression and protein synthesis with age. Proc Natl Acad Sci USA 117, 15581–15590 (2020). [PubMed: 32576685]
62. Powers RW, Kaeberlein M, Caldwell SD, Kennedy BK & Fields S Extension of chronological life span in yeast by decreased TOR pathway signaling. Genes Dev 20, 174–184 (2006). [PubMed: 16418483]
63. Fabrizio P, Pozza F, Pletcher SD, Gendron CM & Longo VD Regulation of longevity and stress resistance by Sch9 in yeast. Science 292, 288–290 (2001). [PubMed: 11292860]
64. Kaeberlein M et al. Regulation of yeast replicative life span by TOR and Sch9 in response to nutrients. Science 310, 1193–1196 (2005). [PubMed: 16293764]
65. David DC et al. Widespread protein aggregation as an inherent part of aging in C. elegans. PLoS Biol 8, e1000450 (2010). [PubMed: 20711477]
66. Barros GC et al. Rqc1 and other yeast proteins containing highly positively charged sequences are not targets of the RQC complex. J Biol Chem 296, 100586 (2021). [PubMed: 33774050]

Additional References

67. Brenner S The genetics of Caenorhabditis elegans. Genetics 77, 71–94 (1974). [PubMed: 4366476]
68. Winzeler EA et al. Functional characterization of the S. cerevisiae genome by gene deletion and parallel analysis. Science 285, 901–906 (1999). [PubMed: 10436161]
69. Yofe I et al. One library to make them all: streamlining the creation of yeast libraries via a SWAp-Tag strategy. Nat Chem Biol 13, 371–378 (2016).
70. Huh W-K et al. Global analysis of protein localization in budding yeast. Nature 425, 686–691 (2003). [PubMed: 14562095]
71. Hughes AL & Gottschling DE An early age increase in vacuolar pH limits mitochondrial function and lifespan in yeast. 492, 261–265 (2012).
72. Ingolia NT, Brar GA, Rouskin S, McGeachy AM & Weissman JS The ribosome profiling strategy for monitoring translation in vivo by deep sequencing of ribosome-protected mRNA fragments. Nat Protoc 7, 1534–1550 (2012). [PubMed: 22836135]
73. Langmead B, Trapnell C, Pop M & Salzberg SL Ultrafast and memory-efficient alignment of short DNA sequences to the human genome. Genome Biol 10, R25 (2009). [PubMed: 19261174]
74. Love MI, Huber W & Anders S Moderated estimation of fold change and dispersion for RNA-seq data with DESeq2. Genome Biol 15, 550 (2014). [PubMed: 25516281]
75. Dey KK, Xie D & Stephens M A new sequence logo plot to highlight enrichment and depletion. BMC Bioinformatics 19, 473 (2018). [PubMed: 30526486]
76. Burtner CR, Murakami CJ, Kennedy BK & Kaeberlein M A molecular mechanism of chronological aging in yeast. cc 8, 1256–1270 (2009).
77. Huang DW, Sherman BT & Lempicki RA Systematic and integrative analysis of large gene lists using DAVID bioinformatics resources. Nat Protoc 4, 44–57 (2009). [PubMed: 19131956]
78. McCormick MA et al. A Comprehensive Analysis of Replicative Lifespan in 4,698 Single-Gene Deletion Strains Uncovers Conserved Mechanisms of Aging. Cell Metabolism 22, 895–906 (2015). [PubMed: 26456335]

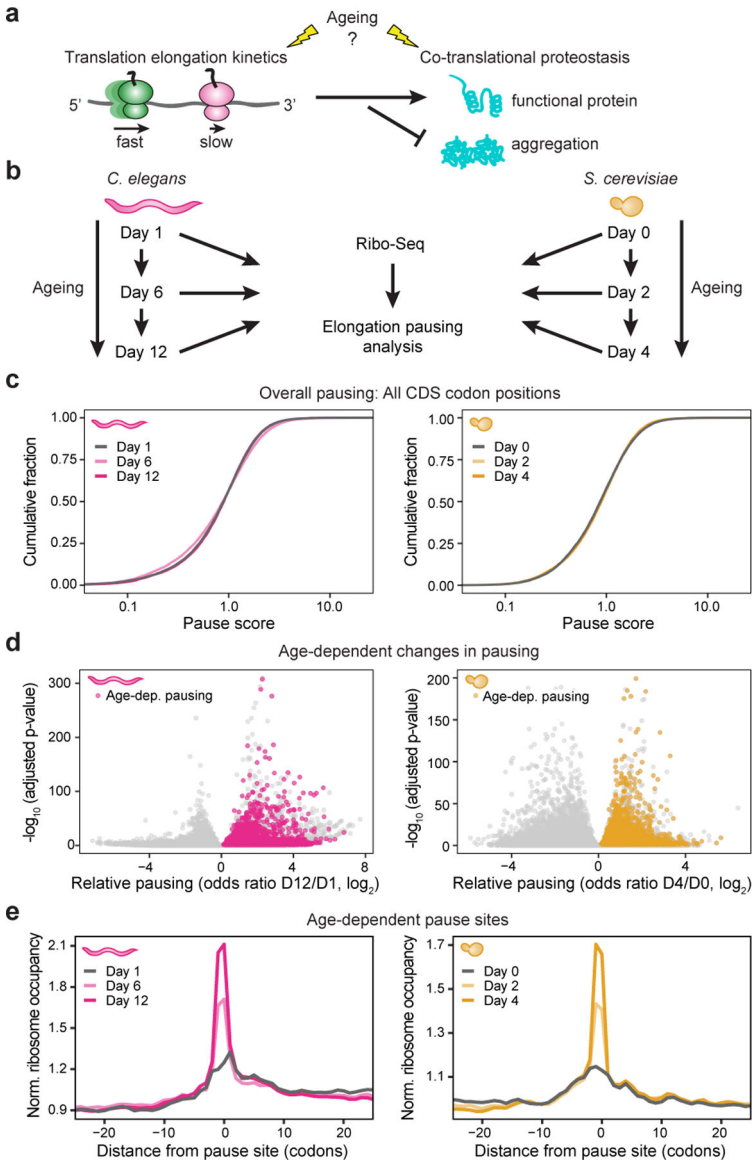

Figure 1. Age-dependent ribosome pausing is conserved.

a, Investigating the impact of ageing on translation kinetics and co-translational proteostasis. **b,** Procedure overview. **c,** Cumulative frequency histogram of pause scores in coding sequences of worms (left) and yeast (right). **d,** Volcano plot of relative ribosome pausing. Colored points indicate codon positions in Day 12 adult worms and Day 4 yeast with significantly increased age-dependent pausing (odds ratio > 1, adjusted $p < 0.05$, two-sided Fisher's Exact test, Benjamini-Hochberg correction), all other translatome positions in grey. **e,** Average ribosome occupancy at age-dependent pause sites, $n = 5{,}503$ sites in 1,282 genes in worms (left), 5,600 sites in 890 genes in yeast (right).

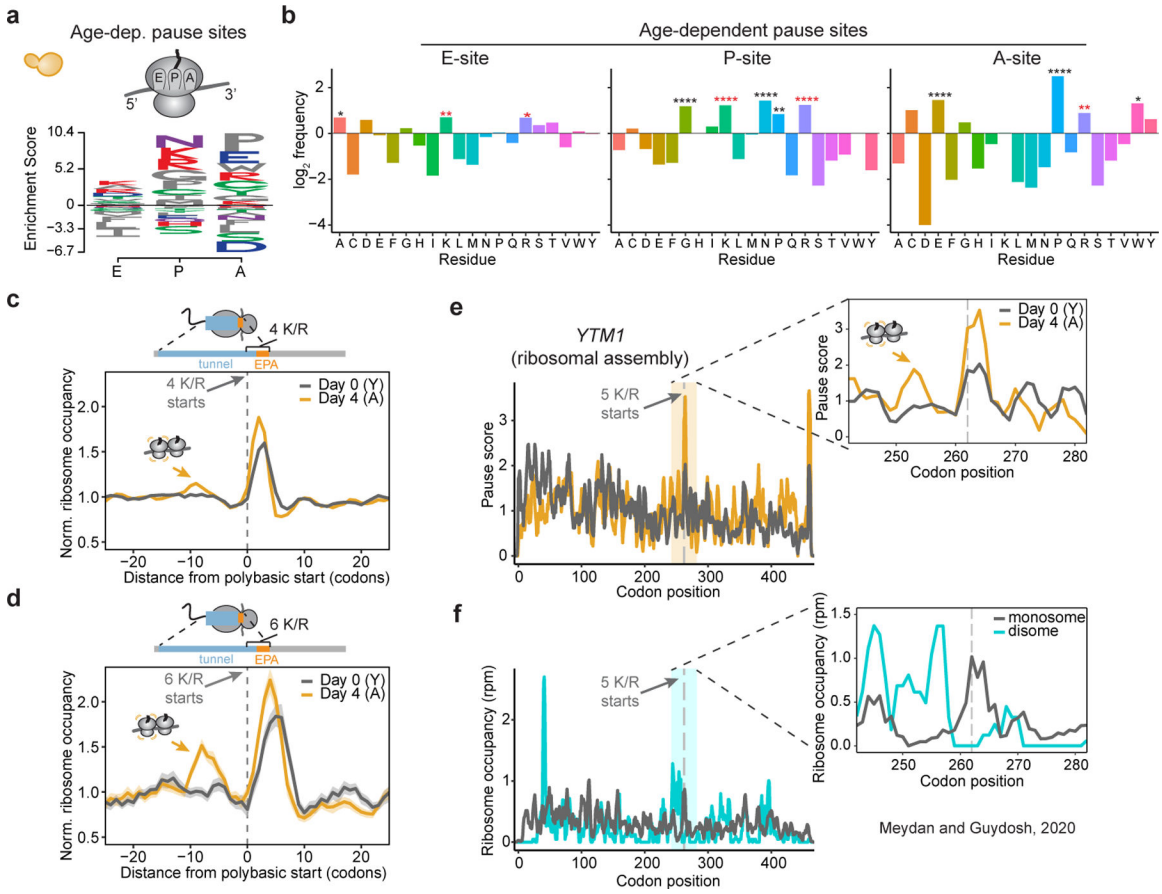

Figure 2. Ageing exacerbates ribosome pausing at polybasic regions in yeast.

a – b, Peptide motif and **b,** amino acid frequencies associated with age-dependent pause sites (n = 271 sites with Day 4 pause score > 6 in 232 genes). *p < 0.05, **p < 0.01, ****p < 1e^{-4}, two-sided Fisher's exact test, with basic residues highlighted. **c,** Average ribosome occupancy at polybasic regions with 4 consecutive Lys/Arg (K/R) for young (Y) Day 0 and aged (A) Day 4 yeast. n = 738 K/R sites in 606 genes. Shaded region represents the 95% bootstrapped confidence interval. Arrow indicates putative ribosome collisions. **d,** As in **c,** for polybasic regions with 6 consecutive K/R. n = 60 sites in 58 genes. **e,** Ribosome occupancy on *YTM1* with inset highlighting pausing and collision (arrow) at 5 consecutive K/R. **f,** Occupancy of monosomes and disomes on *YTM1* from disome profiling of young cells[47].

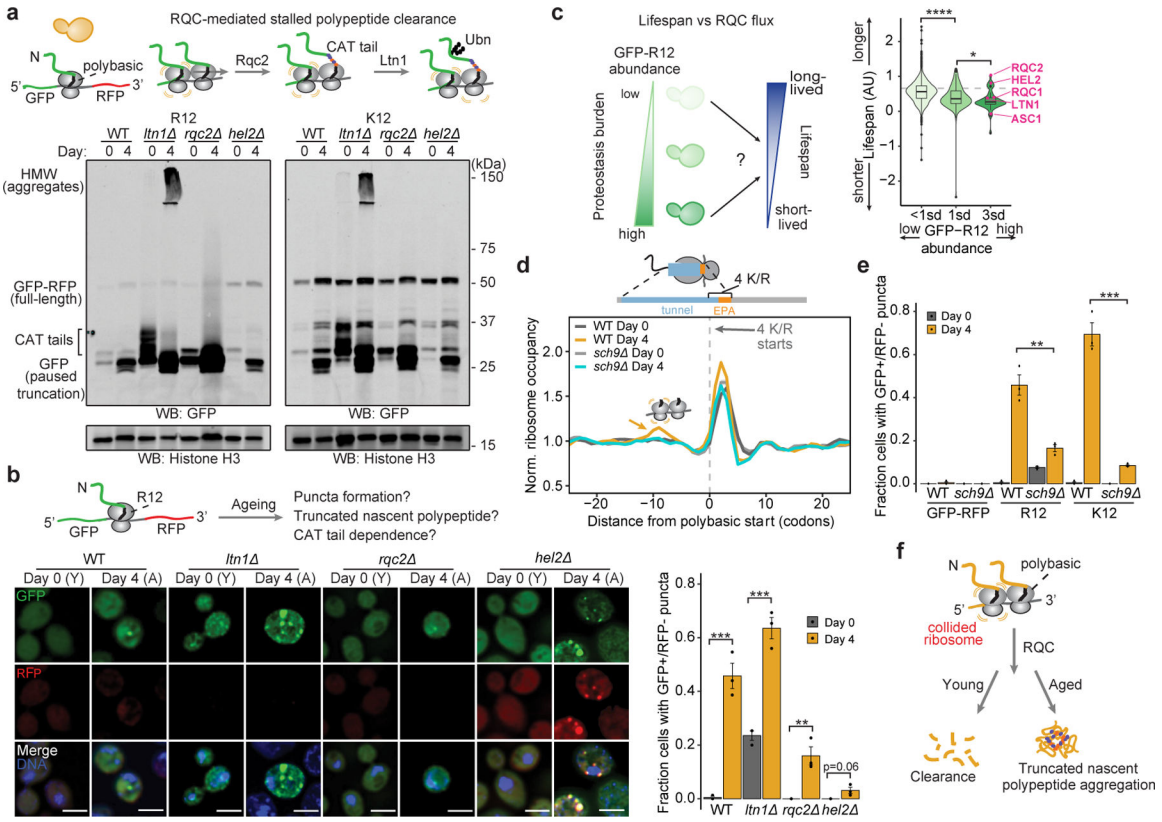

Figure 3. Polybasic-driven age-dependent aggregation of truncated nascent polypeptides in yeast is mitigated in lifespan extension models.

a, Immunoblot of young and aged WT and RQC mutant strains harboring reporters with 12 R or K between *GFP-RFP*. Truncated, full-length, and high-molecular weight (HMW) products are noted. $n \geq 3$ biological replicates with representative example shown. For gel source data, see Supplementary Figure 1. **b,** Fluorescence microscopy and quantification of GFP+/RFP- puncta formation in cells harboring the R12 reporter. $n \geq 3$ biological replicates with representative example shown, $n \geq 200$ cells with mean ± SEM. WT: $p = 6.6e^{-4}$, *ltn1Δ*: $p = 7.6e^{-4}$; *rqc2Δ*: $p = 8.9e^{-3}$, two-sided Welch's *t*-test. Scale bar: 3 μm. **c,** Investigating the association between lifespan and RQC by analyzing the lifespan distribution[62] of the yeast deletion collection based on the abundance of the *GFP-R12-HIS3* reporter[6]. < 1 sd (standard deviation): strains with GFP abundance < 1 sd of the total collection ($n = 4{,}195$); 1 sd: strains with GFP abundance > 1 sd and < 3 sd ($n = 172$); > 3 sd: strains with GFP abundance greater than 3 sd ($n = 39$). Grey line indicates average lifespan of the population. RQC mutants are noted. ****$p = 6.6e^{-13}$, *$p = 0.05$, two-sided Wilcoxon rank-sum test. **d,** Average ribosome occupancy in WT and *sch9Δ* yeast at regions with 4 consecutive K/R. $n = 728$ K/R sites in 598 genes. Shaded region represents the 95% bootstrapped confidence interval. Arrow indicates putative ribosome collisions. **e,** Quantification of GFP+/RFP- puncta formation in WT and *sch9Δ* cells. $n \geq 200$ cells, 3 biological replicates with mean ± SEM; ns: not significant, **$p = 0.004$, ***$p = 0.0004$, two-sided Welch's *t*-test. Scale bar: 3 um. **f,** Proposed model highlighting age-dependent aggregation of truncated nascent polypeptides after a ribosome pausing event.

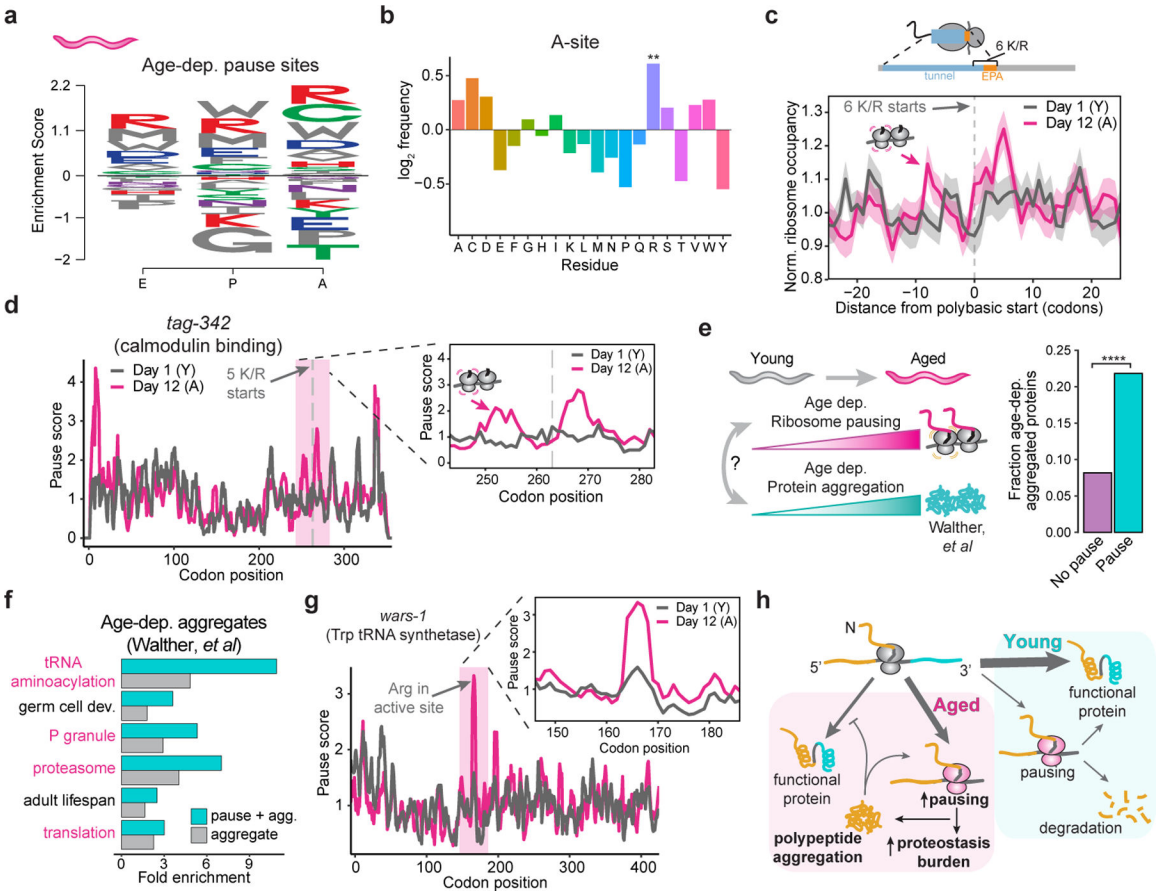

Figure 4. Conserved mechanisms of age-dependent ribosome pausing and aggregation in worms.

a – b, Peptide motif and **b,** ribosomal A-site amino acid frequencies associated with age-dependent pause sites (n = 587 sites with pause score > 10 in 437 genes). **p = 0.005, two-sided Fisher's exact test. **c,** Average ribosome occupancy at polybasic regions with 6 consecutive K/R. n = 109 K/R sites in 100 genes. Shaded region represents the 95% bootstrapped confidence interval. Arrow indicates putative ribosome collisions. **d,** Ribosome occupancy on *tag-342* with inset highlighting pausing and collision (arrow) at 5 consecutive K/R. **e,** Investigating the association between age-dependent ribosome pausing and aggregation[37]. Population n = 742 proteins with a pause site, 6,219 proteins without a pause site. $p = 5.6e^{-22}$, two-sided Fisher's exact test. **f,** Comparing the functional enrichment within aggregated proteins[37] to those that also have age-dependent ribosome pausing, displaying representative gene ontology terms (adjusted $p < 0.05$). Categories related to proteostasis are highlighted. See Supplementary Table 2 for unfiltered results. **g,** Ribosome occupancy on *wars-1* (Trp tRNA synthetase) with inset highlighting pausing at a position with Arg in the ribosomal active site. **h,** Proposed model of increased ribosome pausing and aggregation of truncated nascent polypeptides during ageing.